SIAM J. NUMER. ANAL.
Vol. 61, No. 5, pp. 2352–2380

A POSTERIORI ERROR ESTIMATES FOR DISCONTINUOUS GALERKIN METHODS ON POLYGONAL AND POLYHEDRAL MESHES*

ANDREA CANGIANI†, ZHAONAN DONG‡, AND EMMANUIL H. GEORGOULIS§

Abstract. We present a new residual-type energy-norm a posteriori error analysis for interior penalty discontinuous Galerkin (dG) methods for linear elliptic problems. The new error bounds are also applicable to dG methods on meshes consisting of elements with very general polygonal/polyhedral shapes. The case of simplicial and/or box-type elements is included in the analysis as a special case. In particular, for the upper bounds, an arbitrary number of very small faces is allowed on each polygonal/polyhedral element, as long as certain mild shape-regularity assumptions are satisfied. As a corollary, the present analysis generalizes known a posteriori error bounds for dG methods, allowing in particular for meshes with an arbitrary number of irregular hanging nodes per element. The proof hinges on a new conforming recovery strategy in conjunction with a Helmholtz decomposition formula. The resulting a posteriori error bound involves jumps on the tangential derivatives along elemental faces. Local lower bounds are also proven for a number of practical cases. Numerical experiments are also presented, highlighting the practical value of the derived a posteriori error bounds as error estimators.

Key words. discontinuous Galerkin, a posteriori error bound, polygonal/polyhedral meshes, polytopic elements, irregular hanging nodes

MSC codes. 65N30, 65M60, 65J10

DOI. 10.1137/22M1516701

1. Introduction.

Recent years have witnessed extensive activity in the development of various Galerkin methods posed on meshes consisting of general polygonal/polyhedral (henceforth collectively referred to as *polytopic*) elements. A central question that has arisen is the derivation of computable error bounds for such discretizations, so that the extreme geometric flexibility of such meshes can be harnessed.

Residual-type a posteriori error bounds for interior penalty discontinuous Galerkin (dG) methods on composite/polytopic meshes appeared in [30, 21]. Also, in the context of virtual element methods, corresponding bounds are proven in [14, 19], while for the weak Galerkin approach, an a posteriori error analysis can be found in [39]. In addition, corresponding results for the hybrid high-order method can be found in [24]. All aforementioned results are proven for shape-regular polytopic meshes, under the additional assumption that the diameters of elemental faces are of comparable size to the element diameter. Although the latter may be a reasonable assumption in the context of standard, simplicial meshes, it can be rather restrictive for general polytopic elements. This is because general polygons/polyhedra with more than d

*Received by the editors August 18, 2022; accepted for publication (in revised form) July 5, 2023; published electronically October 17, 2023.
https://doi.org/10.1137/22M1516701

†SISSA, International School for Advanced Studies, I-34136 Trieste, Italy (andrea.cangiani@sissa.it).

‡Inria, 75589, Paris, France, and CERMICS, Ecole des Ponts, 77455, Marne-la-Vallée, France (zhaonan.dong@inria.fr).

§The Maxwell Institute for Mathematical Sciences and Department of Mathematics, School of Mathematical and Computer Sciences, Heriot-Watt University, Edinburgh, EH14 4AS, UK, Department of Mathematics, School of Applied Mathematical and Physical Sciences, National Technical University of Athens, Zografou, 15780, Greece, and IACM-FORTH, Greece (E.Georgoulis@hw.ac.uk).

faces can simultaneously be shape-regular and contain *small* faces, i.e., faces whose diameter is arbitrarily small compared to the element diameter.

This work aims exactly at rectifying this restrictive state of affairs. We prove new energy-norm a posteriori upper error bounds for interior penalty discontinuous dG methods posed on meshes containing polytopic elements, including with an arbitrary number of small faces, as long as certain mild shape-regularity assumptions are satisfied. The case of simplicial and/or box-type elements is included in the analysis as a special case. For accessibility, we restrict the discussion to a model elliptic problem, noting, nevertheless, that various generalizations are possible with minor modifications.

As a general principle, residual-based a posteriori error analysis of nonconforming and, in particular, dG methods requires a recovery of the numerical solution into a related conforming function. The pioneering work of Karakashian and Pascal [35] (see also [34]) proposed the recovery of the dG solution by a nodal averaging operator for which a crucial stability result was proven [35, Theorem 2.2]; cf. also [34, Theorem 2.1] for an extension. This construction allowed for the first rigorous a posteriori error analysis of a dG method for elliptic problems. A number of related results followed, improving various aspects of the theory; for instance, see [3, 33, 18, 46, 1, 8, 32, 23, 37]. A key reason for the aforementioned restrictive assumption that all elemental faces are of comparable size to the element diameter in existing a posteriori error analysis for polytopic dG methods [30, 21] is exactly the lack of availability of a stability result corresponding to [35, Theorem 2.2] for polytopic element meshes containing elements with small faces.

In this work, we crucially avoid the use of averaging operators. Instead, the proof of the upper error bound hinges on a new recovery into H^1-conforming functions, in conjunction with a Helmholtz decomposition. To complete the analysis, we also require the existence of appropriate auxiliary simplicial meshes on which quasi-interpolants are defined. This can be verified in practice using simple and efficient algorithms. We provide two such algorithms, one based on a submesh and one employing tools from computational geometry and, in particular, constrained Delaunay triangulations [20, 43]. The resulting a posteriori error bound involves also jumps on the tangential derivatives along elemental faces.

Local lower bounds are also proven for a number of practical cases, indicating the optimality of the new estimators. The key challenge in the proof of the latter is, again, the treatment of small/degenerating element faces and the construction of respective bubble functions. In particular, local lower bounds for the element residuals are proven allowing for arbitrarily small faces. Lower bounds for the flux residuals are proven under more restrictive assumptions (see Assumption 4.6 below), allowing, nevertheless, for arbitrarily small faces.

We note that the case of meshes consisting of simplicial and/or box-type elements is included in the analysis as a special case. For such "classical" mesh concepts, the developments presented below provide a new class of a posteriori error bounds applicable even to *hp*-version dG methods, allowing in particular for meshes with an arbitrary number of irregular hanging nodes per element.

The remainder of this work is structured as follows. In section 2, we define the elliptic model problem, the admissible meshes, and finite element spaces and the interior penalty dG method on polytopic meshes. We also prove some important technical results regarding the construction of auxiliary meshes which will be instrumental in the proof of a posteriori error bounds. In section 3, we prove the a posteriori upper error bound, using the aforementioned technical developments, while in section 4 we

provide respective lower bounds for the energy-norm error for a number of practical cases. Finally, in section 5, we present some numerical experiments confirming the robustness and efficiency of the derived a posteriori error bound and highlighting its practical value as an error estimator.

2. Model problem and numerical method. For a Lipschitz domain $\omega \subset \mathbb{R}^d$, $d = 1, 2, 3$, we denote by $H^s(\omega)$ the Hilbertian Sobolev space of index $s \geq 0$ of real-valued functions defined on ω, endowed with the seminorm $|\cdot|_{H^s(\omega)}$ and norm $\|\cdot\|_{H^s(\omega)}$. Furthermore, we let $L_p(\omega)$, $p \in [1, \infty]$, be the standard Lebesgue space on ω, equipped with the norm $\|\cdot\|_{L_p(\omega)}$. In the case $p = 2$, we shall simply write $\|\cdot\|_\omega$ to denote the L_2-norm over ω and simplify this further to $\|\cdot\|$ when $\omega = \Omega$, the physical domain. Finally, $|\omega|$ denotes the d-dimensional Hausdorff measure of ω.

2.1. Model problem. Let Ω be a bounded, simply connected, and open polygonal/polyhedral domain in $\mathbb{R}^d$, $d = 2, 3$. The boundary $\partial\Omega$ of Ω is split into two disjoint parts Γ_{D} and Γ_{N} with $|\Gamma_{\mathrm{D}}| \neq 0$. For technical reasons, when $d = 3$ and $|\Gamma_{\mathrm{N}}| \neq 0$, the interface between Γ_{D} and Γ_{N} is assumed that is made up of straight planar segments. We consider the linear elliptic problem: find $u \in H^1(\Omega)$, such that

$$\begin{aligned} -\nabla \cdot (a\nabla u) &= f && \text{in } \Omega, \\ u &= g_{\mathrm{D}} && \text{on } \Gamma_{\mathrm{D}}, \\ a\nabla u \cdot \boldsymbol{n} &= g_{\mathrm{N}} && \text{on } \Gamma_{\mathrm{N}}, \end{aligned} \tag{2.1}$$

with known $f \in L_2(\Omega)$, $g_{\mathrm{D}} \in H^{1/2}(\Gamma_{\mathrm{D}})$, and $g_{\mathrm{N}} \in L_2(\Gamma_{\mathrm{N}})$ and symmetric diffusion tensor $a \in [L_\infty(\Omega)]^{d\times d}$ such that

$$\alpha^*|\xi|^2 \geq \xi^\top a(x)\xi \geq \alpha_*|\xi|^2 > 0 \quad \forall \xi \in \mathbb{R}^d, \quad \text{a.e.} \quad x \in \Omega, \tag{2.2}$$

for some constants $\alpha^*, \alpha_* > 0$. For simplicity of the presentation, we assume that a is piecewise constant, although this is not an essential restriction for the validity of the developments below.

Setting $H^1_{\mathrm{D}} := \{v \in H^1(\Omega) : v = 0 \text{ on } \Gamma_{\mathrm{D}}\}$, the weak formulation of (2.1) is as follows: find $u \in H^1(\Omega)$, $u = g_{\mathrm{D}}$ on Γ_{D} such that

$$\int_\Omega a\nabla u \cdot \nabla v \,\mathrm{d}\mathbf{x} = \int_\Omega fv \,\mathrm{d}\mathbf{x} + \int_{\Gamma_{\mathrm{N}}} g_{\mathrm{N}} v \,\mathrm{d}s \tag{2.3}$$

for all $v \in H^1_{\mathrm{D}}(\Omega)$. The well-posedness is guaranteed by the Lax–Milgram lemma.

2.2. Finite element spaces and trace operators. We consider meshes $\mathcal{T}$ consisting of general polygonal (for $d = 2$) or polyhedral (for $d = 3$) mutually disjoint open elements $K \in \mathcal{T}$, henceforth termed collectively as *polytopic,* with $\cup_{K\in\mathcal{T}} \bar{K} = \bar{\Omega}$. Given $h_K := \mathrm{diam}(K)$, the diameter of $K \in \mathcal{T}$, we define the mesh function $\boldsymbol{h} : \cup_{K\in\mathcal{T}} K \to \mathbb{R}_+$ by $\boldsymbol{h}|_K = h_K$, $K \in \mathcal{T}$. Further, we let $\Gamma := \cup_{K\in\mathcal{T}} \partial K$ denote the mesh skeleton and set $\Gamma_{\mathrm{int}} := \Gamma \backslash \partial\Omega$. The mesh skeleton Γ is decomposed into $(d-1)$-dimensional simplices F denoting the mesh *faces,* shared by at most two elements. These are distinct from elemental *interfaces,* which are defined as the simply connected components of the intersection between the boundary of an element and either a neighboring element or $\partial\Omega$. As such, an interface between two elements may consist of more than one face, separated by hanging nodes/edges shared by those two elements only. This includes both "classical" hanging nodes, typically created by local mesh refinement, and nonstandard ones separating non-coplanar faces. The

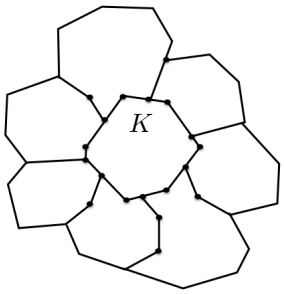

FIG. 1. *Element $K \in \mathcal{T}$ with its facewise neighbors; hanging nodes are highlighted by bullets.*

latter may be created, for instance, by a mesh agglomeration procedure; we refer the reader to Figure 1 for an illustration for $d = 2$.

The *finite element space* $S_{\mathcal{T}}$ with respect to $\mathcal{T}$ is defined by

$$S_{\mathcal{T}} \equiv S_{\mathcal{T}}^p := \{u \in L_2(\Omega) : u|_K \in \mathcal{P}_p(K), K \in \mathcal{T}\}$$

for some $p \in \mathbb{N}$ with $\mathcal{P}_p(K)$ denoting the space of d-variate polynomials of total degree up to p on K. We stress that the local elemental polynomial spaces employed within $S_{\mathcal{T}}$ are defined in the *physical coordinate system,* i.e., without mapping from a given reference or canonical frame. This approach allows us to retain the full local approximation properties of the underlying finite element space. We refer the reader to [13, 12] for a detailed discussion on the benefits and implementation issues resulting from this choice.

Let K_i and K_j be two adjacent elements of $\mathcal{T}$ sharing a face $F \subset \partial K_i \cap \partial K_j \subset \Gamma_{\text{int}}$. For v and $\boldsymbol{q}$ elementwise continuous scalar- and vector-valued functions, respectively, we define the *average* across F by $\{\!\{v\}\!\}|_F := \frac{1}{2}(v|_{F\cap K_i} + v|_{F\cap K_j})$, $\{\!\{\boldsymbol{q}\}\!\}|_F := \frac{1}{2}(\boldsymbol{q}|_{F\cap K_i} + \boldsymbol{q}|_{F\cap K_j})$, respectively, and the *jump* across F by $[\![v]\!] := v|_{F\cap K_i} - v|_{F\cap K_j}$, $[\![\boldsymbol{q}]\!] := \boldsymbol{q}|_{F\cap K_i} - \boldsymbol{q}|_{F\cap K_j}$, using the convention $i > j$ in the element numbering to determine the sign. On a boundary face $F \subset \Gamma_{\text{D}}$, with $F \subset \partial K_i$, $K_i \in \mathcal{T}$, we set $\{\!\{v\}\!\} := v_i$, $\{\!\{\boldsymbol{q}\}\!\} := \boldsymbol{q}_i$, $[\![v]\!] := v_i$, and $[\![\boldsymbol{q}]\!] := \boldsymbol{q}_i$, respectively.

For $v \in S_{\mathcal{T}}$ we denote by $\nabla_h v$ the elementwise gradient; namely, $(\nabla_h v)|_K := \nabla(v|_K)$ for all $K \in \mathcal{T}$. Also, we denote by $\nabla_{\text{T}} v$ the facewise tangential gradient operator acting on the traces of v on Γ, noting that $\nabla_{\text{T}} v$ is double-valued on Γ_{int}. With a slight abuse of notation, we use the same symbol to denote the tangential gradient of boundary functions such as the Dirichlet datum g_{D}.

2.3. Mesh assumptions, inverse inequalities, and approximation results. Each mesh $\mathcal{T}$ is required to conform to the problem data in the following basic way. First, $\mathcal{T}$ must represent exactly the domain, namely $\cup_{K\in\mathcal{T}} K = \Omega$, and be consistent with the subdivision of $\partial\Omega$ into Γ_{D} and Γ_{N}. Moreover, we require resolution of multiscale features of the domain, such as complex boundaries and bottlenecks. Note that, in the context of polytopic meshes, such resolution is not intrinsic in that multiscale geometrical features can be represented by relatively "large" elements with "small" faces. Hence we assume that the local mesh size of each mesh $\mathcal{T}$ is comparable to the local finest scale of Ω. It is clear that such saturation-type assumptions can always be satisfied, possibly after a finite number of refinements of an original coarse mesh. Further, we require the following general polytopic mesh regularity assumption.

Assumption 2.1 (mesh regularity). We assume that each mesh $\mathcal{T}$ satisfies the following mesh regularity conditions. For each $K \in \mathcal{T}$ the following hold:

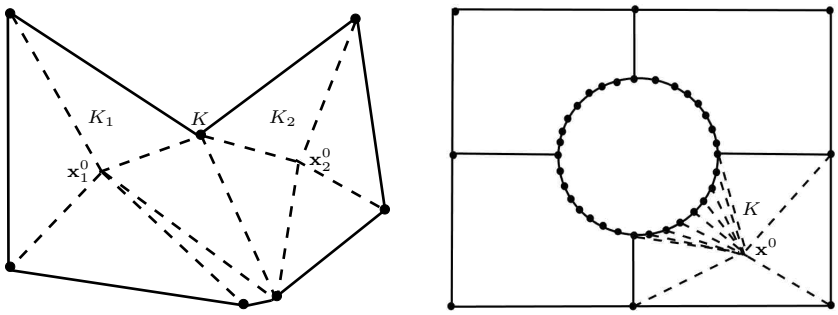

FIG. 2. *Left panel: A polygonal element K with 7 nodes is subdivided into two polygons K_1 and K_2 which are star-shaped with respect to the points $\mathbf{x}_1^0$ and $\mathbf{x}_2^0$, respectively. Right panel: A patch of polygonal elements. The element K has 12 nodes and is star-shaped with respect to a ball centered in $\mathbf{x}^0$.*

(a) K is star-shaped with respect to an inscribed ball of radius $r_K \geq \tau^{-1} h_K$, centered at some point $\mathbf{x}^0 \equiv \mathbf{x}_K^0 \in K$; see Figure 2 (right panel) for an illustration when $d = 2$.
(b) Each face $F \subset \partial K \cap \partial\Omega$ is star-shaped with respect to a $(d-1)$-dimensional ball of radius $r_F \geq \tau^{-1} h_K$.

Here, $\tau > 1$ is a constant independent of the discretization parameters. In what follows, we assume that the centers of the inscribed balls are selected to be chosen so that τ is as minimal.

Remark 2.2. All results below generalize immediately to meshes containing polytopic elements that are finite unions of star-shaped polytopes; see Figure 2 (left panel) for an example. The minimal modifications required in the proofs are detailed in Remark 2.10 below.

Assumption 2.1 allows for very general element shapes, including nonconvex polytopes with an arbitrary number of degenerating faces, i.e., element faces $F \subset \partial K$ with $|F| << h_K^{d-1}$. Notable examples of acceptable subdivisions comprise elements with a bounded number of possibly degenerate hanging nodes and elements with "many" faces obtained by agglomeration of very fine triangulations of the problem domain. Note, however, that Assumption 2.1(b) forbids degenerating/shape-irregular elemental faces on the boundary. This restriction can be relaxed to some extent at the expense of introducing unknown/hard-to-estimate constants, as discussed in Remark 3.7 below.

To the best of our knowledge, Assumption 2.1 allows for the most general polytopic meshes for which a posteriori error bounds are proven, for any Galerkin discretization and for any PDE problem. Nevertheless, it is, perhaps inevitably, more restrictive compared to the respective ones required for stability and a priori error analysis of dG methods; see [11], [12, section 4], and [10] for details. The key advantage of the present setting is that it allows us to be as explicit as possible in the constants involved in the a posteriori error bounds.

We also require the following standard local quasi-uniformity assumption.

Assumption 2.3 (local quasi-uniformity). Each mesh $\mathcal{T}$ is locally quasi-uniform, i.e., there exists a constant $\rho > 0$ such that $\rho^{-1} \leq h_{K_i}/h_{K_j} \leq \rho$, whenever $K_i, K_j \in \mathcal{T}$ share a common face.

We now state and prove a few results stemming from the above shape-regularity and local quasi-uniformity assumptions. A first, geometrical, consequence is that the number of interface neighbors of each $K \in \mathcal{T}$ is, in fact, bounded.

LEMMA 2.4. *Under Assumptions* 2.1 *and* 2.3*, the number of interface neighbors of each element of* $\mathcal{T}$ *is uniformly bounded.*

Proof. Denote by ω_K the set of elements in $\mathcal{T}$ which are neighbors of K. We derive a rough upper-bound on the cardinality n of ω_K as follows. If $K' \in \omega_K$, then $K' \subset B_{h_K+h_{K'}}(\mathbf{x}_K^0) \subseteq B_{(1+\rho)h_K}(\mathbf{x}_K^0)$ thanks to Assumption 2.3. On the other hand, Assumption 2.1 implies that K' contains the ball $B_{r_{K'}}(\mathbf{x}_{K'}^0)$ with $r_{K'} \geq \tau^{-1} h_{K'}$. Letting $C_2 := \pi$ and $C_3 := 4\pi/3$, we thus have $|K'| \geq C_d r_{K'}^d \geq C_d \tau^{-d} h_{K'}^d \geq C_d \tau^{-d} \rho^{-d} h_K^d$. Therefore, $n(C_d \tau^{-d} \rho^{-d} h_K^d) \leq C_d (1+\rho)^d h_K^d$, or $n \leq \tau^d \rho^d (1+\rho)^d$, thereby showing that the number of neighbors of K is uniformly bounded as required. ∎

In particular, the presence of "many small" faces is allowed if these are grouped into a few interfaces only; see Figure 2 (right panel) for an example. Complex interfaces may be produced by agglomeration procedures used to perform numerical upscaling of complex domains described through very fine triangulations [5, 12, 40] or within adaptive algorithms to align the mesh to solution features and coefficient anisotropies [27, 12, 15]

LEMMA 2.5. *Let* $K \in \mathcal{T}$ *satisfying Assumption* 2.1*. Then, for all* $v \in H^1(\Omega)$*, we have the trace estimate*

$$\|v\|_{\partial K}^2 \leq C_{\mathrm{tr}} \left(\frac{\zeta}{h_K} \|v\|_K^2 + \frac{h_K}{\zeta} \|\nabla v\|_K^2 \right) \tag{2.4}$$

for any $\zeta > 0$ *and* C_{tr} *a positive constant only depending on* τ *and on* d*.*

Also, for each $v \in \mathcal{P}_p(K)$*, the inverse estimate*

$$\|v\|_{\partial K}^2 \leq \frac{C_{\mathrm{inv}}}{h_K} \|v\|_K^2 \tag{2.5}$$

holds with $C_{\mathrm{inv}} := \tau(p+1)(p+d)$*.*

Proof. These estimates are special cases of the corresponding ones presented in [10]. The trace estimate (2.4) follows from [10, Lemma 4.7] in conjunction with Assumption 2.1, while (2.5) follows from [10, Lemma 4.4] along with Assumption 2.1. ∎

LEMMA 2.6. *Given* $K \in \mathcal{T}$ *satisfying Assumption* 2.1*, for each* $v \in H^1(K)$*,* $K \in \mathcal{T}$*, we have the bounds*

$$\|v - \Pi_0 v\|_K \leq C_{PF} h_K \|\nabla v\|_K \tag{2.6}$$

and

$$\|v - \Pi_0 v\|_{\partial K} \leq \tilde{C}_{PF} \sqrt{h_K} \|\nabla v\|_K, \tag{2.7}$$

with $\Pi_0 : L_2(\Omega) \to S_{\mathcal{T}}^0$*, the orthogonal* L_2*-projection onto* $S_{\mathcal{T}}^0$*, the space of elementwise constants; here* $C_{PF}, \tilde{C}_{PF} > 0$ *depend on* d *and on* τ *only.*

Proof. The key technical difficulty is to show that C_{PF} and $\tilde{C}_{PF}$ are independent of the shape of K. Under Assumption 2.1, for $K \in \mathcal{T}$ we can apply the Poincaré–Friedrichs inequalities proven in [50, Theorem 3.5] and [47, Proposition 2.10], with

explicit dependence on the shape-regularity constant τ and dimension d, yielding (2.6). Then, (2.7) follows using the trace inequality (2.4). ∎

A crucial technical aspect of the analysis below is the availability of a shape-regular, auxiliary triangulation defined as follows.

DEFINITION 2.7 (auxiliary mesh). *Given the sequence of meshes $\mathcal{T}$, we name as the auxiliary mesh a corresponding sequence of conforming simplicial meshes $\widehat{\mathcal{T}}$ satisfying for each $\widehat{\mathcal{T}}$ and $T \in \widehat{\mathcal{T}}$*

(a) *(shape-regularity) the radius r_T of the largest circle inscribed in T is such that $r_T \geq \widehat{\tau}^{-1} h_T$, where h_T denotes the diameter of T;*
(b) *(local mesh-size compatibility) if $K \in \mathcal{T}$ is such that $K \cap T \neq \emptyset$, it holds that $\widehat{\rho}^{-1} \leq h_T/h_K \leq \widehat{\rho}$,*

with $\widehat{\tau}, \widehat{\rho} > 1$ constants independent of the discretization parameters.

An immediate consequence of the above definition is that, if $\widehat{\mathcal{T}}$ is an auxiliary mesh sequence, then the number of intersections of each $T \in \widehat{\mathcal{T}}$ with the elements of the corresponding polytopic mesh $\mathcal{T}$ is uniformly bounded as a function of the shape-regularity and local quasi-uniformity constants of both the polytopic and auxiliary meshes. The proof of this fact follows along the lines of that of Lemma 2.4.

We note that the evaluation of the error estimator presented below does *not* require the construction of auxiliary meshes in practice. As long as their existence can be assumed, the a posteriori error bound holds. Moreover, we do not expect such an assumption to limit in any possible way the configurations of very general polytopic mesh sequences allowed by Assumptions 2.1 and 2.3. Rather, the issue is to show that auxiliary meshes tightly close to the polytopic meshes can be constructed in principle. To this end, we present two possible algorithms for the construction of auxiliary meshes which apply to progressively complicated primal mesh configurations. Both algorithms are easily and cheaply implementable. As such, if desired, the corresponding auxiliary mesh quality parameters may be computed in practice, thus permitting the explicit evaluation of their impact on the a posteriori error bound.

2.3.1. Auxiliary submesh. Assume that the mesh $\mathcal{T}$ is *fully shape-regular* in the sense that, for each $K \in \mathcal{T}$, each face $F \in \partial K$ satisfies the shape-regularity property which is stated in Assumption 2.1(b) for boundary faces. Then, an auxiliary mesh can be simply constructed by joining F to $\mathbf{x}_K^0$, the center of star-shapedness of $K \in \mathcal{T}$, for each $K \in \mathcal{T}$ and $F \in \partial K$. This approach can be extended to the more general case in which every interface can be replaced by a shape-regular triangulated surface which does not compromise the shape-regularity of the neighboring elements. For instance, any of the four circular interfaces appearing in Figure 2 (right panel) may be replaced by the segment joining its endpoints. This will result in the *auxiliary submesh* shown in Figure 3 (left panel).

2.3.2. Constrained Delauney auxiliary mesh. Auxiliary submeshes are in general not obvious to construct, and, moreover, employing a submesh is not possible when the element faces are shape-irregular and/or of arbitrarily small size with respect to the elemental size. In this case, it is necessary to consider auxiliary meshes which are not logically submeshes of the corresponding polytopic meshes. One possibility, designed to maximize shape-regularity while maintaining the auxiliary mesh as close as possible to the polytopic mesh in terms of local mesh size, is to exploit the concept of *constrained Delaunay triangulations,* introduced in [20] for $d = 2$ and generalized to any d in [43]; see also [26, 44]. We recall their definition, limiting ourselves to the

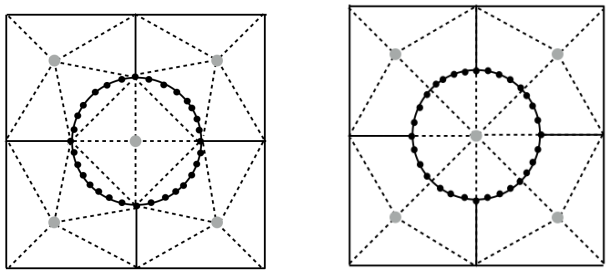

FIG. 3. *A mesh with* 5 *elements (solid lines) and associated auxiliary meshes (dashed lines). Left panel: Auxiliary submesh with* 24 *elements. Right panel: Auxiliary constrained Delauney mesh with* 16 *elements. The dual nodes belonging to the set* $\mathcal{P}$ *of Definition* 2.7 *are marked with grey bullets.*

case of interest, namely when the constraints are given by the mesh faces lying on the boundary of Ω.

DEFINITION 2.8 (constrained Delaunay triangulation). *Let* $\mathcal{X} = \{\mathcal{P}, \mathcal{F}\}$ *with* $\mathcal{P}$ *a set of points in* $\Omega \subset \mathbb{R}^d$ *and* $\mathcal{F}$ *the set of boundary faces of the mesh* $\mathcal{T}$*. A constrained Delaunay triangulation (CDT) associated to* $\mathcal{X}$ *is a triangulation of* Ω*, which conforms to* $\mathcal{F}$*, has* $\mathcal{P}$ *as its set of internal vertices, and satisfies the following constrained Delaunay property: for every* $k \in \{1, \dots, d\}$ *and every* k*-dimensional simplex* S *in the triangulation which is not on* $\partial\Omega$*, there exists a circle* $\mathcal{C}$ *such that*

(1) *the vertices of* S *are on the boundary of* $\mathcal{C}$*;*
(2) *if a vertex* P *of the CDT is in the interior of* $\mathcal{C}$*, then the straight line connecting* P *to at least one of the vertices of* S *intersects* $\partial\Omega$*. (Then, we say that* P *cannot be seen from one of the vertices of* S*.)*

This definition generalizes the concept of Delaunay triangulations in that, if no constraints are given, it would coincide with the definition of Delaunay triangulations. Moreover, as Delaunay triangulations, CDTs maximize the minimum angle among all triangulations generated by the cloud of points $\mathcal{P}$ and constrained by $\mathcal{F}$. The existence of CDTs is analyzed in [20, 43, 44]: CDTs always exists for $d = 2$ while for $d = 3$ they exist if any ridge formed by $\mathcal{F}$ is *strongly Delaunay.* A simplex is strongly Delaunay if the circle $\mathcal{C}$ of Definition 2.8 does not *enclose* any other point in $\mathcal{X}$. As shown in [43, 44], this condition can always be satisfied, possibly after the insertion of a finite number of regular nodes on nonstrongly Delaunay ridges in the skeleton of $\mathcal{F}$. Moreover, once every boundary edge is strongly Delaunay, the restriction of the CDT on each interface is Delaunay.

Given the polytopic mesh $\mathcal{T}$, here we consider the CDT of Ω with seeds $\mathcal{P} = \{\mathbf{x}_K^0\}_{K \in \mathcal{T}}$, possibly after the modification of $\mathcal{F}$ discussed above. We refer the reader to Figure 3 (right panel) for an illustration.

Remark 2.9. We expect the CDTs associated to $\mathcal{T}$ to always satisfy the auxiliary mesh Definition 2.7 owing to their shape-regularity maximization property and the fact that the seeds in $\mathcal{P}$ are well distanced by assumption. However, due to the extreme generality of $\mathcal{T}$, proving this fact appears to be challenging and would result in overly pessimistic estimation of the shape-regularity and quasi-uniformity constants. Specifically, the difficulty comes from the contrasting requirements of shape-regularity and local mesh size compatibility, due to which an element of the CDT may overlap with elements of $\mathcal{T}$ which are not direct neighbors; see Figure 4 (right panel) for an

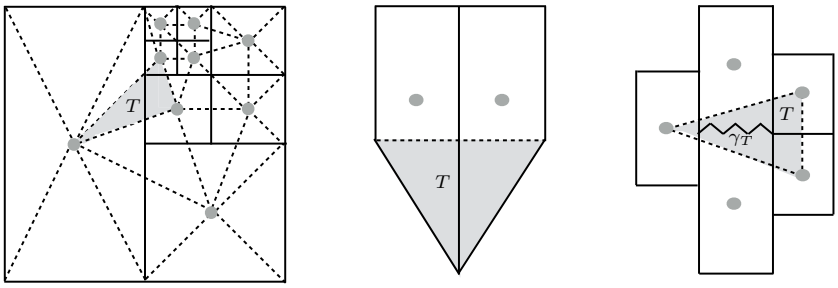

FIG. 4. *Constrained Delauney auxiliary mesh examples. Different configurations for the set* Γ_T *of* (2.10) *for the auxiliary element* T *marked in grey. Left:* $\Gamma_T = \Gamma_T^{\mathrm{c}}$. *Center:* $\Gamma_T = \Gamma_T^{\mathrm{o}}$. *Right:* Γ_T^{o} *is made of a single interface* γ_T, *while the rest of* Γ_T *belongs to* Γ_T^{c}. *The simplices required in the proof of Lemma* 2.13 *to estimate the contributions from each edge in* γ_T *partially overlap (not shown).*

example. Hence, in the a posteriori error analysis below, we have opted for keeping the requirements of Definition 2.7 as an assumption which can be verified economically and sharply in practice. Indeed, contrary to auxiliary submeshes, CDTs can always be constructed, and their construction is, in fact, simpler in general. If desired, their qualitative parameters may be easily evaluated using well-established and efficient algorithms [20, 43, 44].

Remark 2.10. In the case of meshes with elements made of finite unions of star-shaped subpolytopes, auxiliary meshes should be constructed starting from the centers of the subpolytopes instead. The results below still hold as long as local quasi-uniformity is assumed for the submesh comprising the star-shaped subpolytopes.

2.3.3. Auxiliary mesh interpolation and inverse estimates. We recall the following Scott–Zhang-type quasi-interpolation result [42, 41, 48, 17].

LEMMA 2.11 (quasi-interpolant). *Let* $\widehat{\mathcal{T}}$ *be a shape-regular simplicial subdivision of* Ω *not containing any hanging nodes. Then, there exists a quasi-interpolation operator* $I_h : H^1(\Omega) \to H^1(\Omega) \cap S^1_{\widehat{\mathcal{T}}}$, *such that*

$$\|v - I_h v\|_T + h_T \|\nabla(v - I_h v)\|_T \leq C_{\mathrm{sz}} h_T \|\nabla v\|_{\omega_T}, \tag{2.8}$$

where ω_T *denotes the patch of elements in* $\widehat{\mathcal{T}}$ *with nonempty intersection with* $\overline{T}$. *The constant* $C_{\mathrm{sz}} > 0$ *depends only on the shape-regularity constant* $\widehat{\tau}$ *of the auxiliary mesh* $\widehat{\mathcal{T}}$. *If the function* v *has nonhomogeneous piecewise linear trace on* $\partial\Omega$, *we have* $I_h v|_F = v|_F$ *for all* $F \subset \partial T \cap \partial\Omega$, $T \in \widehat{\mathcal{T}}$.

Moreover, we have

$$\|v - I_h v\|^2_{\partial K} \leq C_{\mathrm{in}} h_K \|\nabla v\|^2_{\widehat{\omega}_K}, \tag{2.9}$$

with $C_{\mathrm{in}} > 0$ *depending only on the shape-regularity of* $\mathcal{T}$ *and of* $\widehat{\mathcal{T}}$. *Here,* $\widehat{\omega}_K = \cup\{\omega_T : T \cap K \neq \emptyset, T \in \widehat{\mathcal{T}}\}$.

Proof. The proof of (2.8) can be found in [42, 41, 48, 17] for various levels of generality. Noting that (2.9) refers to the trace on the skeleton of the *original* polytopic mesh, we apply the trace inequality (2.4) with $\zeta = 1$,

$$\begin{aligned}\|v - I_h v\|^2_{\partial K} &\leq C_{\mathrm{tr}} \left(h_K^{-1} \|v - I_h v\|^2_K + h_K \|\nabla(v - I_h v)\|^2_K\right) \\ &\leq C_{\mathrm{tr}} \sum_{T \in \widehat{\mathcal{T}} : T \cap K \neq \emptyset} \left(h_K^{-1} \|v - I_h v\|^2_T + h_K \|\nabla(v - I_h v)\|^2_T\right),\end{aligned}$$

and (2.9) follows from (2.8), depending on the shape-regularity of $\mathcal{T}$ through C_{tr} and on the shape-regularity of $\widehat{\mathcal{T}}$ through (2.8). ∎

The next polynomial inverse estimation result, relating L_2-norms on subsets of the mesh skeleton Γ of $\mathcal{T}$ with L_2-norms over elements of the auxiliary mesh $\widehat{\mathcal{T}}$, will be important for the analysis below. In this context, for each $T \in \widehat{\mathcal{T}}$, we consider the set of *cut interfaces* obtained by the intersection of Γ with the simplex T, which we characterize as follows:

$$\Gamma_T := \Gamma \cap T = \Gamma_T^{\mathrm{c}} \cup \Gamma_T^{\mathrm{o}}, \tag{2.10}$$

with Γ_T^{c} the set of interfaces $\gamma_T \in \Gamma_T \cap \Omega$ such that $\gamma_T \subset \partial K$ with K an element of $\mathcal{T}$ whose center of star-shapedness is a vertex of T, and $\Gamma_T^{\mathrm{o}} := \Gamma_T \setminus \Gamma_T^{\mathrm{c}}$. Note that the number of interfaces in Γ_T is bounded since the number of intersections of T with the elements $K \in \mathcal{T}$ is bounded; however, each such interface may be made of an arbitrary number of cut faces, due to the complexity of the intersecting polytopic elements.

The subdivision in (2.10) reflects increasing levels of difficulty, with Γ_T^{o} collecting complex interfaces for which the proof of the inverse estimate is more challenging. As usual, the proof rests in employing simplices obtained by joining each face composing Γ_T with the most appropriate vertex of T and summing up all contributions. When $\Gamma_T^{\mathrm{o}} \neq \emptyset$, such simplices may overlap. In this case, the constant of the resulting inverse estimate depends on the number of such overlaps and thus reflects the complexity of Γ_T. The complex interface γ_T highlighted in Figure 4 (right panel) provides an example in which this eventuality may occur.

Remark 2.12. In the case of submesh auxiliary meshes, we always have $\Gamma_T^{\mathrm{o}} = \emptyset$. Instead, for constrained Delauney auxiliary meshes, $\Gamma_T^{\mathrm{o}} \neq \emptyset$ in general; we refer the reader to Figure 4 for some examples.

LEMMA 2.13. *Let Assumptions* 2.1 *and* 2.3 *hold, and let $\widehat{\mathcal{T}}$ be an auxiliary mesh related to $\mathcal{T}$. Given $q \in \mathbb{N}$, for all $T \in \widehat{\mathcal{T}}$ and $v \in \mathcal{P}_q(T)$, we have*

$$\|v\|_{\Gamma_T}^2 \leq \frac{\widehat{C}_{\mathrm{inv}}}{h_T} \|v\|_T^2. \tag{2.11}$$

The constant $\widehat{C}_{\mathrm{inv}}$ depends on d, q, and on shape-regularity and local quasi-uniformity of both $\mathcal{T}$ and $\widehat{\mathcal{T}}$ only. If $\Gamma_T \equiv \Gamma_T^{\mathrm{c}}$, then $\widehat{C}_{\mathrm{inv}} = \tau(q+1)(q+d)$. If $\Gamma_T^{\mathrm{o}} \neq \emptyset$, $\widehat{C}_{\mathrm{inv}}$ depends also on the number of overlaps n_{o} required to cover the elements of Γ_T^{o}; cf. (2.13). *In particular, if $\Gamma_T^{\mathrm{o}} \subset \partial\Omega$, then $n_{\mathrm{o}} \leq d$.*

Proof. We consider Γ_T^{c} and Γ_T^{o} separately, starting with Γ_T^{c}. Exploiting the star-shapedness property of Γ_T^{c} with respect to the vertices of T, which is inherited from Assumption 2.1, the inverse inequality

$$\|v\|_{\Gamma_T^{\mathrm{c}}}^2 \leq \frac{\tau(q+1)(q+d)}{h_T} \|v\|_T^2$$

follows in the same way as (2.5).

Considering now the set Γ_T^{o}, we observe that each cut interface belonging to Γ_T^{o} may be partitioned into a set of $(d-1)$-dimensional simplices. Indeed, each interface inherits a set of, possibly cut, simplicial faces from Γ. If a face $F \in \Gamma$ is only partially contained in Γ_T^{o}, then $F \cap T$ is still an interval if $d = 2$ while it can always be subdivided into four triangles if $d = 3$. Let now $\widehat{F}$ be one such $(d-1)$-dimensional simplex within Γ_T^{o}. We note that, if a simplex T has inradius r_T, then, for any

given intersecting hyperplane Z, there exists a vertex V of T such that $d(V,Z)\geq r$. Otherwise, S must be contained in the region $\{\mathbf{x}\in\mathbb{R}^d : d(\mathbf{x},Z)<r\}$, in contradiction with the fact that T contains a (closed) ball of radius r. It follows that we can always construct a nondegenerate simplex $T_{\widehat{F}}$ by joining $\widehat{F}$ with a vertex V of T such that $d(V,\widehat{F})\geq r$. We thus have (cf. (2.5)) the inverse estimate:

$$\|v\|^2_{\widehat{F}} \leq \widehat{\tau}\frac{(q+1)(q+d)}{h_T}\|v\|^2_{T_{\widehat{F}}} \qquad \forall v\in\mathcal{P}_q(T). \tag{2.12}$$

Then, summing up over all $\widehat{F}\in\Gamma_T^{\mathrm{o}}$, we conclude that

$$\|v\|^2_{\Gamma_T^{\mathrm{o}}} \leq \frac{\widehat{\tau}(q+1)(q+d)}{h_T}\sum_{\widehat{F}\in\Gamma_T^{\mathrm{o}}}\|v\|^2_{T_{\widehat{F}}} \leq n_{\mathrm{o}}\frac{\widehat{\tau}(q+1)(q+d)}{h_T}\|v\|^2_T, \tag{2.13}$$

with n_{o} the number of overlaps of the simplices $T_{\widehat{F}}$, $\widehat{F}\in\Gamma_T^{\mathrm{o}}$. In particular, if Γ_T^{o} is only made of boundary interfaces, then $n_{\mathrm{o}}\leq d$, as there may be at most d such interfaces, each made of a single $(d-1)$-dimensional simplex. The required estimate now follows by summing up the contributions from Γ_T^{c} and Γ_T^{o}. ∎

Remark 2.14. The constant $\widehat{C}_{\mathrm{inv}}$ appearing in (2.11) accounts for the complexity of the mesh in terms of topology and shape, quantified by the number n_{o} of overlap required to cover the mesh skeleton; see the mesh shown in Figure 4 (right) for an illustrative example. In typical practical cases, e.g., meshes stemming from standard algorithms such as Voronoi tessellations, as well as shape-regular adaptively generated meshes, we expect to have $\Gamma_T\equiv\Gamma_T^{\mathrm{c}}$ for the vast majority of auxiliary elements. For instance, for the adaptively refined mesh with multiple hanging nodes shown Figure 4 (left), Γ_T^{o} either is empty or contains a single boundary edge, i.e., no overlaps are required, resulting in the "ideal" constant $\widehat{C}_{\mathrm{inv}}=\tau(q+1)(q+d)$ for each $T\in\widehat{\mathcal{T}}$.

2.4. Discontinuous Galerkin method. Let $\mathcal{V}:=S_{\mathcal{T}}+H^1(\Omega)$. The symmetric interior penalty dG method reads as follows: find $u_h\in S_{\mathcal{T}}$ such that

$$B(u_h,v_h)=\ell(v_h) \qquad \text{for all} \quad v_h\in S_{\mathcal{T}}, \tag{2.14}$$

whereby $B(\cdot,\cdot):\mathcal{V}\times\mathcal{V}\to\mathbb{R}$ is defined by

$$\begin{aligned} B(w,v) := &\int_\Omega a\nabla_h w\cdot\nabla_h v\,\mathrm{d}\mathbf{x} + \int_{\Gamma\setminus\Gamma_{\mathrm{N}}}\sigma[\![w]\!][\![v]\!]\,\mathrm{d}s,\\ &-\int_{\Gamma\setminus\Gamma_{\mathrm{N}}}(\{\!\{a(\boldsymbol{\Pi}\nabla w)\cdot\boldsymbol{n}\}\!\}[\![v]\!]+\{\!\{a(\boldsymbol{\Pi}\nabla v)\cdot\boldsymbol{n}\}\!\}[\![w]\!])\,\mathrm{d}s, \end{aligned} \tag{2.15}$$

for $w,v\in\mathcal{V}$, and $\ell(\cdot):\mathcal{V}\to\mathbb{R}$ by

$$\ell(v):=\int_\Omega fv\,\mathrm{d}\mathbf{x}-\int_{\Gamma_{\mathrm{D}}}g_{\mathrm{D}}\big((a(\boldsymbol{\Pi}\nabla v))\cdot\boldsymbol{n}-\sigma v\big)\,\mathrm{d}s+\int_{\Gamma_{\mathrm{N}}}g_{\mathrm{N}}v\,\mathrm{d}s,$$

with $\boldsymbol{\Pi}:[L_2(\Omega)]^d\to[S_{\mathcal{T}}]^d$ denoting the orthogonal L_2-projection operator onto the (vectorial) finite element space, and $\sigma\in L_\infty(\Gamma\setminus\Gamma_{\mathrm{N}})$ being the so-called *discontinuity-penalization function* given by

$$\sigma(\mathbf{x}):=\begin{cases} C_\sigma\max\limits_{K\in\{K_i,K_j\}}\Big\{\dfrac{\bar{a}_K C_{\mathrm{inv}}}{h_K}\Big\}, & \mathbf{x}\in F\in\Gamma_{\mathrm{int}},\ F\subseteq\partial K_i\cap\partial K_j,\\[2ex] C_\sigma\dfrac{\bar{a}_K C_{\mathrm{inv}}}{h_K}, & \mathbf{x}\in F\in\Gamma_{\mathrm{D}},\ F\subset\partial K, \end{cases} \tag{2.16}$$

with C_σ a positive constant and $\bar{a}_K := |\sqrt{a}|_2^2|_K$, $K \in \mathcal{T}$; here $|\cdot|_2$ denotes the natural matrix-l_2-norm. The known dependence of the penalty on the local polynomial degree is included in C_{inv} for brevity; see [12, 10] for details. Note that, using (2.3) and that $[\![v]\!] = 0$ on $\Gamma \backslash \Gamma_{\mathrm{N}}$ for all $v \in H^1_{\mathrm{D}}$, we have $B(u,v) = \ell(v)$ for all $v \in H^1_{\mathrm{D}}$, with $u \in H^1(\Omega)$ the solution to (2.3).

Remark 2.15. To avoid further notational overhead, we opted in exposing the main results for elementwise constant diffusion tensors, i.e., $a \in (S^{\mathbf{0}}_{\mathcal{T}})^{d\times d}$, and for the classical interior penalty dG method. With minor modifications, the results below can also be extended to more general coefficients. Moreover, we expect that a corresponding analysis to what is presented below holds also for the interior penalty dG variants from [29, 25].

Upon defining the dG norm by $|||v||| := \left(\|\sqrt{a}\nabla_h v\|^2 + \|\sqrt{\sigma}[\![v]\!]\|^2_{\Gamma\backslash\Gamma_{\mathrm{N}}}\right)^{1/2}$, we have the following result.

LEMMA 2.16. *Under Assumption* 2.1*, there exists* $C_\sigma > 0$*, such that*

$$B(v,v) \geq C_{\mathrm{coer}}|||v|||^2 \quad \textit{and} \quad B(w,v) \leq C_{\mathrm{cont}}|||w|||\,|||v||| \quad \textit{for all} \quad v \in \mathcal{V}, \tag{2.17}$$

respectively, with $C_{\mathrm{coer}}, C_{\mathrm{cont}} > 0$*, independent of* h *of* p*, and* $K \in \mathcal{T}$*.*

We refer the reader to [12, 10] for the proof and the explicit definition of C_σ. A priori error bounds are also available [12, 10].

3. A posteriori error analysis. The following analysis requires Assumptions 2.1 and 2.3 and that an auxiliary mesh according to Definition 2.8 is given.

We decompose the error into two components:

$$e = u - u_h = (u - u_c) + (u_c - u_h) =: e_c + e_d,$$

whereby $u_c \in H^1(\Omega)$ is the recovery of the discrete solution $u_h \in S_{\mathcal{T}}$, defined by

$$B(u_c, v) = B(u_h, v) \qquad \forall v \in H^1_{\mathrm{D}}(\Omega), \tag{3.1}$$

and $u_c = g_{\mathrm{D}}$ on Γ_{D}. The existence and uniqueness of u_c are guaranteed by the Lax–Milgram lemma.

Remark 3.1. The construction of u_c is known in the theory of finite element methods and has been used in various contexts, e.g., in [28] for the design of equilibrated flux a posteriori error estimators and in [45] for the analysis of domain decomposition preconditioners. A crucial reason of using this recovery instead of the averaging operator as in [35] is that it is essentially independent of the mesh geometry and topology; this is clearly helpful in the present context of very general polytopic meshes.

3.1. Bounding the nonconforming error e_d. Inspired by [22, 16] (cf. also [6, 9]), we decompose the nonconforming error $e_d = u_c - u_h$ further via a Helmholtz decomposition.

LEMMA 3.2. *Given that* Ω *is simply connected, for any* $\boldsymbol{w} \in (L_2(\Omega))^d$*, there exist* $\xi \in H^1_{\mathrm{D}}(\Omega)$ *and* $\phi \in [H^1(\Omega)]^{2d-3}$*,* $d = 2, 3$*, such that*

$$a\mathbf{w} = a\nabla\xi + \operatorname{curl}\phi \quad \textit{in } \Omega, \tag{3.2}$$

and ϕ *can be chosen so that*

$$\operatorname{curl}\phi \cdot \boldsymbol{n} = 0 \quad \textit{on } \Gamma_{\mathrm{N}}. \tag{3.3}$$

Moreover, the following relations hold:

$$\|\sqrt{a}\mathbf{w}\|^2 = \|\sqrt{a}\nabla\xi\|^2 + \|a^{-1/2}\operatorname{curl}\phi\|^2, \tag{3.4}$$

and

$$\|\nabla\phi\| \le C_\Omega \|\operatorname{curl}\phi\|, \tag{3.5}$$

with a constant $C_\Omega > 0$ only depending on Ω.

Proof. The proof of (3.2) is given in [22, Theorem 3.1] for the $d=2$ case and is extended to $d=3$ in [16]. Since $\nabla\xi$ is orthogonal to $\operatorname{curl}\phi$, from the symmetry of the diffusion tensor a, the orthogonality (3.4) follows immediately. Finally, the proof of (3.5) can be found in [16]; for $d=2$, we have $C_\Omega = 1$. ∎

Remark 3.3. The Helmholtz decomposition can be generalized to multiply connected domains [31]. However, concerning the validity in this setting of the relation (3.5), which is fundamental to our analysis, we are only aware of the recent preprint [7]. For this reason, we prefer to limit the current analysis to the simply connected setting, leaving possible extensions to future work.

Condition (3.3) imposes a constraint on Γ_{N} for $\phi \in [H^1(\Omega)]^{2d-3}$. Namely, $\operatorname{curl}\phi \cdot \boldsymbol{n}_F = 0$ on $F \subset \Gamma_{\mathrm{N}}$, implying that $\phi \in [H^1(\Omega)]^3$ has constant components on each $(d-1)$-dimensional planar subset of Γ_{N}.

We apply the Helmholtz decomposition with $\boldsymbol{w} = \nabla_h e_d$. Hence $\xi \in H^1_{\mathrm{D}}(\Omega)$ and $\phi \in [H^1(\Omega)]^{2d-3}$ are such that $a\nabla_h e_d = a\nabla\xi + \operatorname{curl}\phi$, and we have

$$\|\sqrt{a}\nabla_h e_d\|^2 = \int_\Omega a\nabla_h e_d \cdot \nabla\xi \,\mathrm{d}\mathbf{x} + \int_\Omega \nabla_h e_d \cdot \operatorname{curl}\phi \,\mathrm{d}\mathbf{x}. \tag{3.6}$$

Since $u_c \in H^1(\Omega)$ with $u_c|_{\Gamma_{\mathrm{D}}} = g_{\mathrm{D}}$ and $\xi \in H^1_{\mathrm{D}}(\Omega)$, (3.1) implies

$$\int_\Omega a\nabla_h e_d \cdot \nabla\xi \,\mathrm{d}\mathbf{x} = -\int_{\Gamma_{\mathrm{int}}} \{\!\{a(\boldsymbol{\Pi}\nabla\xi)\cdot\boldsymbol{n}\}\!\}[\![u_h]\!]\,\mathrm{d}s - \int_{\Gamma_{\mathrm{D}}} (a(\boldsymbol{\Pi}\nabla\xi)\cdot\boldsymbol{n})(u_h - g_{\mathrm{D}})\,\mathrm{d}s.$$

Hence, using the Cauchy–Schwarz inequality, the trace inverse estimate (2.5), the definition of σ, and the orthogonality (3.4), we have, respectively,

$$\begin{aligned}
&\int_\Omega a\nabla_h e_d \cdot \nabla\xi \,\mathrm{d}\mathbf{x} \\
&\quad\le \|\sigma^{-1/2}\{\!\{a(\boldsymbol{\Pi}\nabla\xi)\}\!\}\|_{\Gamma\setminus\Gamma_{\mathrm{N}}} \Big(\|\sqrt{\sigma}[\![u_h]\!]\|^2_{\Gamma_{\mathrm{int}}} + \|\sqrt{\sigma}(u_h - g_{\mathrm{D}})\|^2_{\Gamma_{\mathrm{D}}}\Big)^{1/2} \\
&\quad\le \Big(C_\sigma{}^{-1} \sum_{K\in\mathcal{T}} \|\boldsymbol{\Pi}(\sqrt{a}\nabla\xi)\|^2_K\Big)^{1/2} \Big(\|\sqrt{\sigma}[\![u_h]\!]\|^2_{\Gamma_{\mathrm{int}}} + \|\sqrt{\sigma}(u_h - g_{\mathrm{D}})\|^2_{\Gamma_{\mathrm{D}}}\Big)^{1/2} \\
&\quad\le (C_\sigma)^{-1/2} \|\sqrt{a}\nabla\xi\| \Big(\|\sqrt{\sigma}[\![u_h]\!]\|^2_{\Gamma_{\mathrm{int}}} + \|\sqrt{\sigma}(u_h - g_{\mathrm{D}})\|^2_{\Gamma_{\mathrm{D}}}\Big)^{1/2} \\
&\quad\le \|\sqrt{a}\nabla_h e_d\| \Big(\|\sqrt{\sigma C_\sigma^{-1}}[\![u_h]\!]\|^2_{\Gamma_{\mathrm{int}}} + \|\sqrt{\sigma C_\sigma^{-1}}(u_h - g_{\mathrm{D}})\|^2_{\Gamma_{\mathrm{D}}}\Big)^{1/2}.
\end{aligned} \tag{3.7}$$

To bound the second term on the right-hand side of (3.6), we first decompose

$$\int_\Omega \nabla_h e_d \cdot \operatorname{curl}\phi \,\mathrm{d}\mathbf{x} = \int_\Omega \nabla_h e_d \cdot \operatorname{curl}(\phi - I_h\phi)\,\mathrm{d}\mathbf{x} + \int_\Omega \nabla_h e_d \cdot \operatorname{curl} I_h\phi \,\mathrm{d}\mathbf{x}, \tag{3.8}$$

with I_h the (componentwise if $d=3$) quasi-interpolation operator of Lemma 2.11.

Starting with the first term, observing that $\operatorname{curl}\nabla u_c = \mathbf{0}$, and using the fact that $\phi \in [H^1(\Omega)]^{2d-3}$ satisfying (3.3), implying that ϕ is a constant function on each planar section of Γ_{N}, and choosing $\phi = I_h\phi$ on Γ_{N}, we have

$$\int_\Omega \nabla u_c \cdot \operatorname{curl}(\phi - I_h\phi)\,\mathrm{d}\mathbf{x} = \int_{\Gamma_{\mathrm{D}}} (\phi - I_h\phi)\nabla_{\mathrm{T}} g_{\mathrm{D}}\,\mathrm{d}s.$$

Applying integration by parts, observing that $\operatorname{curl}\nabla e_d|_K = \mathbf{0}$, and using that $(\phi - I_h\phi)$ is single valued on each face and $(\phi - I_h\phi)_{\Gamma_N} = 0$ yields

$$\begin{aligned}\sum_{K\in\mathcal{T}}\int_K \nabla e_d \cdot \operatorname{curl}(\phi - I_h\phi)\,\mathrm{d}\mathbf{x}\\ &= -\int_\Gamma (\phi - I_h\phi)[\![\nabla_{\mathrm{T}} u_h]\!]\,\mathrm{d}s + \int_{\Gamma_D}(\phi - I_h\phi)\nabla_{\mathrm{T}} g_D\,\mathrm{d}s\\ &= -\int_{\Gamma_{\mathrm{int}}} (\phi - I_h\phi)[\![\nabla_{\mathrm{T}} u_h]\!]\,\mathrm{d}s - \int_{\Gamma_D}(\phi - I_h\phi)\nabla_{\mathrm{T}}(u_h - g_D)\,\mathrm{d}s.\end{aligned} \tag{3.9}$$

Further, using (2.9) and, finally, (3.5) and (3.4), the right-hand side of (3.9) can be further estimated from above by

$$\begin{aligned}&\sum_{K\in\mathcal{T}} \|h_K^{-1/2}(\phi - I_h\phi)\|_{\partial K\setminus\Gamma_N}\left(\|\sqrt{h}_K[\![\nabla_{\mathrm{T}} u_h]\!]\|_{\partial K\cap\Gamma_{\mathrm{int}}} + \|\sqrt{h}_K\nabla_{\mathrm{T}}(u_h - g_D)\|_{\partial K\cap\Gamma_D}\right)\\ &\quad\le \left(\sum_{K\in\mathcal{T}} C_{\mathrm{tr}}C_I\|\nabla\phi\|^2_{\widehat{\omega}_K}\right)^{1/2}\left(\|\sqrt{h}[\![\nabla_{\mathrm{T}} u_h]\!]\|^2_{\Gamma_{\mathrm{int}}} + \|\sqrt{h}\nabla_{\mathrm{T}}(u_h - g_D)\|^2_{\Gamma_D}\right)^{1/2}\\ &\quad\le C_1\|\nabla\phi\|_\Omega\left(\|\sqrt{h}[\![\nabla_{\mathrm{T}} u_h]\!]\|^2_{\Gamma_{\mathrm{int}}} + \|\sqrt{h}\nabla_{\mathrm{T}}(u_h - g_D)\|^2_{\Gamma_D}\right)^{1/2}\\ &\quad\le C_1C_\Omega\sqrt{\alpha^*}\|\sqrt{a}\nabla_h e_d\|\left(\|\sqrt{h}[\![\nabla_{\mathrm{T}} u_h]\!]\|^2_{\Gamma_{\mathrm{int}}} + \|\sqrt{h}\nabla_{\mathrm{T}}(u_h - g_D)\|^2_{\Gamma_D}\right)^{1/2}\end{aligned} \tag{3.10}$$

for C_1 a constant depending only on the shape-regularity constant $\widehat{\tau}$ of the auxiliary mesh $\widehat{\mathcal{T}}$, and on the local quasi-uniformity constants ρ and $\hat{\rho}$.

We now consider the second term in (3.8). Since $I_h\phi \in [H^1(\Omega)]^{2d-3}$, we have $\nabla\cdot\operatorname{curl} I_h\phi = 0$ on Ω and, hence, $[\![\operatorname{curl} I_h\phi\cdot\boldsymbol{n}]\!] = 0$ on Γ_{int}. Moreover, given that $I_h\phi$ is constant on each component of Γ_N, we also have $\operatorname{curl} I_h\phi\cdot\boldsymbol{n} = 0$ on Γ_N. Then, integration by parts and working as above gives

$$\begin{aligned}\int_\Omega \nabla_h e_d\cdot\operatorname{curl} I_h\phi\,\mathrm{d}\mathbf{x} &= \sum_{K\in\mathcal{T}}\int_{\partial K} e_d\boldsymbol{n}_K\cdot\operatorname{curl} I_h\phi\,\mathrm{d}s\\ &= -\int_{\Gamma_{\mathrm{int}}}[\![u_h]\!](\boldsymbol{n}\cdot\operatorname{curl} I_h\phi)\,\mathrm{d}s - \int_{\Gamma_D}(u_h - g_D)(\boldsymbol{n}\cdot\operatorname{curl} I_h\phi)\,\mathrm{d}s.\end{aligned}$$

Next, applying to $I_h\phi$ the trace inverse inequality with respect to the auxiliary mesh $\widehat{\mathcal{T}}$ given in (2.11), we obtain

$$\begin{aligned}&\int_\Omega \nabla_h e_d\cdot\operatorname{curl} I_h\phi\,\mathrm{d}\mathbf{x}\\ &\quad\le \left(\|\sqrt{\sigma}[\![u_h]\!]\|^2_{\Gamma_{\mathrm{int}}} + \|\sqrt{\sigma}(u_h - g_D)\|^2_{\Gamma_D}\right)^{1/2}\left(\sum_{T\in\widehat{\mathcal{T}}}\|\sigma^{-1/2}\operatorname{curl} I_h\phi\|^2_{T\cap(\Gamma\setminus\Gamma_N)}\right)^{1/2}\\ &\quad\le \left(\|\sqrt{\sigma}[\![u_h]\!]\|^2_{\Gamma_{\mathrm{int}}} + \|\sqrt{\sigma}(u_h - g_D)\|^2_{\Gamma_D}\right)^{1/2}\left(\sum_{T\in\widehat{\mathcal{T}}}\widehat{C}_{\mathrm{inv}}h_T^{-1}\|\sigma^{-1/2}\operatorname{curl} I_h\phi\|^2_T\right)^{1/2}\\ &\quad\le C_2\left(\|\sqrt{\sigma C_\sigma^{-1}}[\![u_h]\!]\|^2_{\Gamma_{\mathrm{int}}} + \|\sqrt{\sigma C_\sigma^{-1}}(u_h - g_D)\|^2_{\Gamma_D}\right)^{1/2}\|\operatorname{curl} I_h\phi\|\end{aligned}$$

for $C_2 > 0$ constant depending on C_{inv}, $\widehat{C}_{\mathrm{inv}}$, $\widehat{\rho}$, and on α^*. Next, we use the stability of I_h from Lemma 2.11 together with (3.5) to deduce

$$\|\operatorname{curl} I_h\phi\|_\Omega \le C_c\|\nabla\phi\|_\Omega \le C_cC_\Omega\sqrt{\alpha_*}\|a^{-1/2}\nabla\phi\| \le C_cC_\Omega\sqrt{\alpha_*}\|\sqrt{a}\nabla_h e_d\|. \tag{3.11}$$

Hence, combing (3.7), (3.9), (3.10), and (3.11), we arrive at the bound

$$\begin{aligned}\|\sqrt{a}\nabla_h e_d\|^2 \le C_{\rm nc}\Big(&\|\sqrt{\sigma C_\sigma^{-1}}[\![u_h]\!]\|^2_{\Gamma_{\rm int}} + \|\sqrt{\sigma C_\sigma^{-1}}(u_h - g_{\rm D})\|^2_{\Gamma_{\rm D}}\\ &+ \|\sqrt{h}[\![\nabla_{\rm T} u_h]\!]\|^2_{\Gamma_{\rm int}} + \|\sqrt{h}\nabla_{\rm T}(u_h - g_{\rm D})\|^2_{\Gamma_{\rm D}}\Big);\end{aligned} \tag{3.12}$$

the constant $C_{\rm nc} > 0$ depends on $C_{\rm inv}$, $\widehat{C}_{\rm inv}$, $\widehat{\rho}$, C_Ω, and on α^*, α_*, but is independent of h and the number and measure of the mesh faces.

Remark 3.4. We stress that the mesh size h in (3.12) is the local element diameter for $\mathcal{T}$, i.e., *independent* of the measure of the faces and the number of faces per element. This new bound refines the now classical results in [35] by showing that the dG error has, in fact, two sources: the normal flux and the tangential gradient. By applying the inverse inequality on each face F, the L_2-norm of the tangential jump can be bounded from above by the L_2-norm of the jump term itself, thus recovering the bound in [35]. However, such a bound would be proportional to $\operatorname{diam}(K)/\operatorname{diam}(F)$ for each face $F \in \Gamma$, which may be severely pessimistic for increasingly small faces F.

3.2. Bounding the conforming error e_c. For $v \in H^1_{\rm D}$, we have

$$B(e, v) = \ell(v) - B(u_h, v) = \ell(\eta) - B(u_h, \eta), \tag{3.13}$$

with $\eta := v - v_h$, for any $v_h \in S_{\mathcal{T}}$. Recalling that $e = e_c + e_d$, since $e_c \in H^1_{\rm D}$ we can fix $v = e_c$ in (3.13) to further deduce

$$\|\sqrt{a}\nabla e_c\|^2 = B(e_c, e_c) = (\ell(\eta) - B(u_h, \eta)) - B(e_d, e_c) = \ell(\eta) - B(u_h, \eta), \tag{3.14}$$

from (3.1). The right-hand side of (3.14) can now be bounded via standard arguments [35]: integration by parts, application of [4, eq. (3.3)], the observation that $\boldsymbol{\Pi}\nabla u_h = \nabla u_h$, and elementary manipulations yield

$$\begin{aligned}\ell(\eta) - B(u_h, \eta) = &\int_\Omega (f + \nabla_h \cdot (a\nabla_h u_h))\eta \,{\rm d}\mathbf{x} - \int_{\Gamma_{\rm int}} [\![a\nabla u_h \cdot \boldsymbol{n}]\!]\{\!\{\eta\}\!\}\,{\rm d}s\\ &- \int_{\Gamma_{\rm N}} (a\nabla u_h \cdot \boldsymbol{n} - g_{\rm N})\eta\,{\rm d}s - \int_{\Gamma_{\rm int}} \sigma[\![u_h]\!][\![\eta]\!]\,{\rm d}s - \int_{\Gamma_{\rm D}} \sigma(u_h - g_{\rm D})\eta\,{\rm d}s\\ &+ \int_{\Gamma_{\rm int}} \{\!\{a(\boldsymbol{\Pi}\nabla\eta)\cdot\boldsymbol{n}\}\!\}[\![u_h]\!]\,{\rm d}s + \int_{\Gamma_{\rm D}} \big(a(\boldsymbol{\Pi}\nabla\eta)\cdot\boldsymbol{n}\big)(u_h - g_{\rm D})\,{\rm d}s =: \sum_{i=1}^7 T_i.\end{aligned} \tag{3.15}$$

Setting $\eta = e_c - \Pi_0 e_c$ and using (2.6), we have

$$T_1 \le C_{PF}\alpha_*^{-1/2}\left(\sum_{K\in\mathcal{T}} \|h_K(f + \nabla\cdot(a\nabla u_h)\|^2_K\right)^{1/2} \|\sqrt{a}\nabla e_c\|. \tag{3.16}$$

Employing (2.7), along with standard manipulations, we also have

$$\begin{aligned}T_2 + T_3 \le &\sum_{K\in\mathcal{T}}\sum_{F\subset\partial K\cap\Gamma_{\rm int}} \|h_K^{-1/2}\eta\|_F \|\sqrt{h}_K[\![a\nabla u_h\cdot\boldsymbol{n}]\!]\|_F\\ &+ \sum_{K\in\mathcal{T}}\sum_{F\subset\partial K\cap\Gamma_{\rm N}} \|h_K^{-1/2}\eta\|_F \|\sqrt{h}_K(a\nabla u_h\cdot\boldsymbol{n} - g_{\rm N})\|_F\\ &\le \tilde{C}_{PF}\alpha_*^{-1/2}\|\sqrt{a}\nabla e_c\|\left(\|\sqrt{h}[\![a\nabla u_h\cdot\boldsymbol{n}]\!]\|^2_{\Gamma_{\rm int}} + \|\sqrt{h}(a\nabla u_h\cdot\boldsymbol{n} - g_{\rm N})\|^2_{\Gamma_{\rm N}}\right)^{1/2}.\end{aligned} \tag{3.17}$$

Similarly, using the definition of σ from (2.16), we have

$$\begin{aligned} T_4+T_5 &\le \big(\|\sqrt{\sigma}[\![u_h]\!]\|^2_{\Gamma_{\rm int}}+\|\sqrt{\sigma}(u_h-g_{\rm D})\|^2_{\Gamma_{\rm D}}\big)^{1/2}\|\sigma^{1/2}[\![\eta]\!]\|_{\Gamma\setminus\Gamma_{\rm N}}\\ &\le \left(\sum_{K\in\mathcal{T}}\max_{F\in\partial K\setminus\Gamma_{\rm N}}\sigma\|\eta\|^2_{\partial K\setminus\Gamma_{\rm N}}\right)^{1/2}\big(\|\sqrt{\sigma}[\![u_h]\!]\|^2_{\Gamma_{\rm int}}+\|\sqrt{\sigma}(u_h-g_{\rm D})\|^2_{\Gamma_{\rm D}}\big)^{1/2} \qquad (3.18)\\ &\le \sqrt{C_\sigma\alpha^*/\alpha_*}C_{\rm inv}\tilde{C}_{PF}\rho\|\sqrt{a}\nabla e_c\|\big(\|\sigma^{1/2}[\![u_h]\!]\|^2_{\Gamma_{\rm int}}+\|\sqrt{\sigma}(u_h-g_{\rm D})\|^2_{\Gamma_{\rm D}}\big)^{1/2}. \end{aligned}$$

Now, using the trace inverse estimate (2.5), the stability of the L_2-projection operator, and that $\nabla\eta|_K=\nabla e_c|_K$, we deduce that

$$\begin{aligned} T_6+T_7 &\le \big(\|\sqrt{\sigma}[\![u_h]\!]\|^2_{\Gamma_{\rm int}}+\|\sqrt{\sigma}(u_h-g_{\rm D})\|^2_{\Gamma_{\rm D}}\big)^{1/2}\|\sigma^{-1/2}\{\!\{a(\boldsymbol{\Pi}\nabla e_c)\cdot\boldsymbol{n}\}\!\}\|_{\Gamma\setminus\Gamma_{\rm N}}\\ &\le \Big(\sum_{K\in\mathcal{T}}\max_{F\in\partial K\setminus\Gamma_{\rm N}}\sigma^{-1}\|\sqrt{a}(\boldsymbol{\Pi}(\sqrt{a}\nabla e_c))\cdot\boldsymbol{n}\|^2_F\Big)^{1/2}\\ &\quad\times\big(\|\sqrt{\sigma}[\![u_h]\!]\|^2_{\Gamma_{\rm int}}+\|\sqrt{\sigma}(u_h-g_{\rm D})\|^2_{\Gamma_{\rm D}}\big)^{1/2} \qquad (3.19)\\ &\le C_\sigma^{-1/2}\rho\|\sqrt{a}\nabla e_c\|\big(\|\sqrt{\sigma}[\![u_h]\!]\|^2_{\Gamma_{\rm int}}+\|\sqrt{\sigma}(u_h-g_{\rm D})\|^2_{\Gamma_{\rm D}}\big)^{1/2}. \end{aligned}$$

Hence, by collecting above bounds (3.16), (3.17), (3.18), (3.19), and (3.15), we arrive at the following bound on the conforming error:

$$\begin{aligned} \|\sqrt{a}\nabla e_c\| \le C_{\rm co}\Big(&\|h(f+\nabla_h\cdot(a\nabla_h u_h)\|^2+\|\sqrt{\sigma}[\![u_h]\!]\|^2_{\Gamma_{\rm int}}+\|\sqrt{\sigma}(u_h-g_{\rm D})\|^2_{\Gamma_{\rm D}}\\ &+\|\sqrt{h}[\![a\nabla u_h\cdot\boldsymbol{n}]\!]\|^2_{\Gamma_{\rm int}}+\|\sqrt{h}(a\nabla u_h\cdot\boldsymbol{n}-g_{\rm N})\|^2_{\Gamma_{\rm N}}\Big)^{1/2}, \qquad (3.20)\end{aligned}$$

with $C_{\rm co}$ depending on C_σ, ρ, τ, the polynomial degree p, C_{PF}, and $\tilde{C}_{PF}$, but independent of h and the number and measure of the elemental faces.

We are now ready to present the a posteriori error upper bound.

THEOREM 3.5 (upper bound). *Let u be the solution of (2.1) and let $u_h\in S_{\mathcal{T}}$ be its dG approximation on a polytopic mesh satisfying Assumptions 2.1 and 2.3. Also let an auxiliary mesh according to Definition 2.8 be given. Then, we have the following a posteriori error bound:*

$$|||u-u_h|||^2 \le C_{\rm up}\sum_{K\in\mathcal{T}}(R_K^2+O_K^2), \qquad (3.21)$$

with the local estimator $R_K^2=R_{K,E}^2+R_{K,N}^2+R_{K,J}^2+R_{K,T}^2$, and the data oscillation $O_K^2=O_{K,E}^2+O_{K,N}^2+O_{K,J}^2+O_{K,T}^2$, given by

$$\begin{aligned} R_{K,E}&:=\|h(\Pi f+\nabla\cdot(a\nabla u_h))\|_K,\\ R_{K,N}&:=\big(\|\sqrt{h}[\![a\nabla u_h\cdot\boldsymbol{n}]\!]\|^2_{\partial K\cap\Gamma_{\rm int}}+\|\sqrt{h}(a\nabla u_h\cdot\boldsymbol{n}-\bar{g}_{\rm N})\|^2_{\partial K\cap\Gamma_{\rm N}}\big)^{1/2},\\ R_{K,J}&:=\big(\|\sqrt{\sigma}[\![u_h]\!]\|^2_{\partial K\cap\Gamma_{\rm int}}+\|\sqrt{\sigma}(u_h-\bar{g}_{\rm D})\|^2_{\partial K\cap\Gamma_{\rm D}}\big)^{1/2},\\ R_{K,T}&:=\big(\|\sqrt{h}[\![\nabla_{\rm T}u_h]\!]\|^2_{\partial K\cap\Gamma_{\rm int}}+\|\sqrt{h}\nabla_{\rm T}(u_h-\bar{g}_{\rm D})\|^2_{\partial K\cap\Gamma_{\rm D}}\big)^{1/2},\\ O_{K,E}&:=\|h(f-\Pi f)\|_K,\quad O_{K,N}:=\|\sqrt{h}(g_{\rm N}-\bar{g}_{\rm N})\|_{\partial K\cap\Gamma_{\rm N}},\\ O_{K,J}&:=\|\sqrt{\sigma}(g_{\rm D}-\bar{g}_{\rm D})\|_{\partial K\cap\Gamma_{\rm D}},\quad O_{K,T}:=\|\sqrt{h}\nabla_{\rm T}(g_{\rm D}-\bar{g}_{\rm D})\|_{\partial K\cap\Gamma_{\rm D}}, \end{aligned}$$

with $C_{\rm up}$ depending on $C_{\rm co}$ and $C_{\rm nc}$ only, but independent of h and of the number and measure of the elemental faces; here, for any for $K\in\mathcal{T}$, such that $\partial K\cap\Gamma_S\neq\emptyset$ with $S\in\{D,N\}$, we set $\bar{g}_S|_{\partial K\cap\Gamma_S}\in\mathcal{P}_{p_k}(\partial K\cap\Gamma_S)$ with g_S denoting an approximation of the Dirichlet and Neumann data, respectively.

Proof. The proof follows immediately from the bounds (3.12) and (3.20), together with the triangle inequality $|||u-u_h||| \le |||e_c||| + |||e_d|||$. ∎

Remark 3.6. In the above, we followed a known approach in splitting the estimator into a "residual part" and a "data oscillation part," assuming that $f \in L_2(\Omega)$ and for sufficiently smooth boundary data. In this setting the data oscillation error is typically dominated by the residual estimators. However, if the forcing data $f \in H^{-1}(\Omega)$, then data oscillation may dominate the error [38]. It would be an interesting future development to investigate the approach from [38] in the context of dG methods.

Remark 3.7. Theorem 3.5 has been proven under Assumption 2.1(b) which disallows boundary faces with arbitrarily small size relative to the local mesh size. This assumption is reasonable, as much resolution of the problem domain is required in order for the numerical solution to incorporate the boundary conditions. Nevertheless, this assumption can be relaxed in the case of Dirichlet boundary conditions as follows. Note that the latter is only required to construct the interpolant of the divergence-free component ϕ of the nonconforming error, which is not constrained on the Dirichlet boundary. Thus, the interpolant may be constructed for an extension $\tilde{\phi}$, (e.g., as a Stein-type extension operator) defined on an extended domain $\tilde{\Omega} \supset \Omega$ whose respective mesh $\tilde{\mathcal{T}}$ would correspond "closely" to the primal mesh $\mathcal{T}$ and is constructed so that it may contain *no* small boundary faces. The resulting bounds, however, would depend on the, typically unknown, boundedness constant of the extension operator.

4. Lower bounds.

We now derive lower bounds for the a posteriori error estimator of Theorem 3.5. Of particular interest is the extent to which the efficiency of the estimator can be shown to be independent of the number and of the relative sizes of $(d-1)$-dimensional faces in the mesh. The situation differs for the elemental residual and face jump residuals; for clarity, we deal with them separately.

4.1. Elemental residual.

Lower bounds for the elemental residual can be derived under no further assumptions on the mesh. The analysis is based on a new element bubble function and some auxiliary results.

LEMMA 4.1 ([10, Corollary 4.24]). *Let $\mathcal{T}$ satisfy the Assumption* 2.1. *Then, for each $K \in \mathcal{T}$, $p \in \mathbb{N}$, and $v \in \mathcal{P}_p(K)$, the following inverse inequality holds:*

$$\|\nabla v\|_K^2 \le C_{\mathrm{inv},K} h_K^{-2} \|v\|_K^2, \tag{4.1}$$

with $C_{\mathrm{inv},K}$ a positive constant depending only on d, p, and τ. Note also the trivial inequality $\|\mathrm{curl}\, v\|_K^2 \le (d-1)\|\nabla v\|_K^2$.

Next, for a generic d-dimensional simplex T, we denote its barycentric coordinates by λ_T^i, $d = 0, \dots, d$, and denote by F_i, $i = 0, \dots, d$, the corresponding $(d-1)$-dimensional simplicial face of T such that $\lambda_T^i|_{F_i} = 0$. Note that $\|\nabla \lambda_T^i\|_{L_\infty(T)} = d|F_i|/|T|$, since $\nabla \lambda_T^i$ is constant. Importantly, the maximum norm is determined by the distance of the ith vertex from the face F_i, but it is *independent of the measure of face F_i;* see Figure 5 (left) for an illustration.

Let $K \in \mathcal{T}$ and let m_K be the number of its faces. Given that K is star-shaped by Assumption 2.1, we can construct a nonoverlapping subdivision of K into m_K simplicial subelements τ_j by joining the face F_j, $j = 1, \dots, m_K$, of K with the center of the largest ball inscribed in K; see Figure 5 (right) for an illustration. Note that $h_K \ge \mathrm{diam}(\tau_j) \ge r_K \ge \tau^{-1} h_K$. Moreover, letting $\lambda_j := \lambda_{\tau_j}^i$ with i such that $\lambda_{\tau_j}^i$ is the barycentric coordinate of τ_j corresponding to the vertex of τ_j which is internal to K,

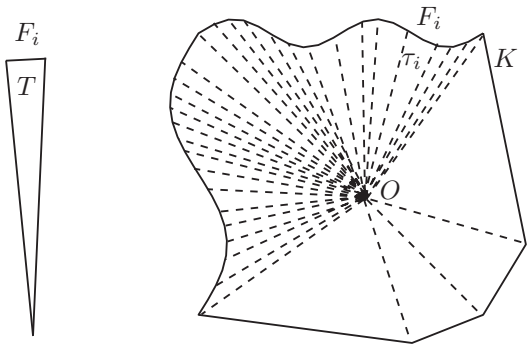

FIG. 5. *Left: A triangle with one "small" face. Right: A polytopic element with many "small" faces.*

it follows that

$$h_K^{-1} \le \|\nabla \lambda_j\|_{L_\infty(\tau_j)} = d|\partial\tau_j \cap \partial K|/|\tau_j| \le \tau h_K^{-1}. \tag{4.2}$$

DEFINITION 4.2 (element bubble). *Let $K \in \mathcal{T}$ and let m_K be the number of its faces. With the above notation, the element bubble function b_K is defined as*

$$b_K|_{\tau_j} = \lambda_j \tag{4.3}$$

for $j = 1, \ldots, m_K$.

By construction, b_K is a continuous piecewise polynomial function with zero trace and with values in $[0, 1]$ on K. Next, we will derive some important properties of the new bubble function (4.3).

LEMMA 4.3. *For each $K \in \mathcal{T}$ satisfying the Assumption* 2.1 *and for each $v \in \mathcal{P}_p(K)$, we have*

$$\|\nabla(b_K v)\|_K^2 \le 2(\tau^2 + C_{\mathrm{inv},K}) h_K^{-2} \|v\|_K^2, \tag{4.4}$$

with τ as in Assumption 2.1 *and $C_{\mathrm{inv},K}$ as in* (4.1)*, and*

$$\|v\|_K^2 \le C_{b,K} \|b_K^{1/2} v\|_K^2, \tag{4.5}$$

with $C_{b,K} := [2(p+2)]^{2d} \frac{d^{d+1}}{(d-1)!}$.

Proof. Using the triangle inequality, the bound (4.2), and the inverse inequality (4.1), we have, respectively,

$$\begin{aligned}
\|\nabla(b_K v)\|_K^2 &\le 2\|(\nabla b_K) v\|_K^2 + 2\|b_K(\nabla v)\|_K^2 \\
&\le 2 \sum_{j=1}^{m_K} \|\nabla \lambda_j\|_{L_\infty(\tau_j)}^2 \|v\|_{\tau_j}^2 + 2\|b_K\|_{L_\infty(K)}^2 \|\nabla v\|_K^2 \\
&\le 2\tau^2 h_K^{-2} \sum_{i=1}^{m_K} \|v\|_{\tau_i}^2 + 2C_{\mathrm{inv},K} h_K^{-2} \|v\|_K^2 = 2(\tau^2 + C_{\mathrm{inv},K}) h_K^{-2} \|v\|_K^2, \qquad (4.6)
\end{aligned}$$

which is the bound required in (4.4). We now prove the norm equivalence relation (4.5). Recalling the norm equivalence relation for each $v \in \mathcal{P}_p(T)$ on a simplex T from [49, section 3.6], we have

$$\|v\|_T^2 \le [2(p+2)]^{2d}\Big(\frac{d}{d+1}\Big)^{d+1}\frac{1}{(d-1)!}\|(\psi_T)^{1/2}v\|_T^2, \tag{4.7}$$

with $\psi_T := (d+1)^{d+1}(\prod_{i=0}^d \lambda_T^i)$. Then, by using $\|\lambda_T^i\|_{L_\infty(T)} = 1$, $i = 0,\dots,d$, we deduce

$$\|v\|_T^2 \le C_{b,K}\|(\lambda_T^i)^{1/2}v\|_T^2 \tag{4.8}$$

for each $i \in \{0,\dots,d\}$. Hence, the bound (4.5) is proven using the definition of $b_K(x)$ in (4.3):

$$\|v\|_K^2 = \sum_{j=1}^{m_K}\|v\|_{\tau_j}^2 \le \sum_{j=1}^{m_K} C_{b,K}\|(\lambda_j)^{1/2}v\|_{\tau_j}^2 = C_{b,K}\|b_K^{1/2}v\|_K^2. \tag{4.9}$$ ∎

Remark 4.4. The new element bubble function on polytopic meshes in the above lemma is different from the classical element bubble function on simplices. In particular, we note that the important relations (4.4) and (4.5) are independent of the number and measure of the faces of the element K.

THEOREM 4.5 (elemental residual lower bound). *Let u be the solution of* (2.1) *and let $u_h \in S_{\mathcal{T}}$ be its dG approximation under Assumptions* 2.1 *and* 2.3. *Then, for each $K \in \mathcal{T}$, we have*

$$\|h(\Pi f + \nabla\cdot(a\nabla u_h))\|_K^2 \le 2C_{b,K}\big(2\big(\tau^2 + C_{\mathrm{inv},K}\big)(\alpha^*)^2\|\sqrt{a}\nabla e\|_K^2 + O_{K,E}^2\big). \tag{4.10}$$

Proof. We fix $v \in H^1_{\mathrm{D}}(\Omega)$ as $v|_K = b_K(\Pi f + \nabla\cdot(a\nabla u_h))$, where b_K is the element bubble function in (4.3), and extended to zero outside K. Using relations (3.13), (3.15), (4.4), and $b_K \le 1$, we obtain

$$\begin{aligned}\int_K b_K(\Pi f + \nabla\cdot(a\nabla u_h))^2\,\mathrm{d}\mathbf{x} &= \int_K (\Pi f - f)v\,\mathrm{d}\mathbf{x} + \int_K a\nabla e\cdot\nabla v\,\mathrm{d}\mathbf{x}\\ &\le \|\Pi f - f\|_K\|v\|_K + \|\sqrt{a}\nabla e\|_K\|\sqrt{a}\nabla v\|_K\\ &\le \big(\|\Pi f - f\|_K + \sqrt{2\big(\tau^2 + C_{\mathrm{inv},K}\big)}\alpha^* h_K^{-1}\|\sqrt{a}\nabla e\|_K\big)\|(\Pi f + \nabla\cdot(a\nabla u_h))\|_K. \end{aligned} \tag{4.11}$$

Recalling (4.5), we have $\|\Pi f + \nabla\cdot(a\nabla u_h)\|_K^2 \le C_{b,K}\|b_K^{1/2}(\Pi f + \nabla\cdot(a\nabla u_h))\|_K^2$ from which the result (4.10) already follows. ∎

4.2. Flux residuals. In view of proving the lower bound for the flux residuals, we require the number of faces of each element to be uniformly bounded. Furthermore, in the case $d = 3$ we shall assume that each face F is shape-regular. Note that such assumptions still allow for arbitrarily small faces.

Assumption 4.6. The number of faces of every element $K \in \mathcal{T}$ is uniformly bounded. For $d = 3$ only, for every $F \in \Gamma_{\mathrm{int}}$, the radius r_F of the largest $(d-1)$-dimensional ball inscribed in F satisfies $r_F \ge \tau^{-1}h_F$, with τ as in Assumption 2.1.

Note that the above assumption does *not* forbid the size of a mesh face to be arbitrarily smaller than that of the elements it belongs to.

To construct the face bubble function, we consider the standard face bubble functions supported in a pair of simplices contained in the neighboring elements.

DEFINITION 4.7 (face bubble). *Let $K \in \mathcal{T}$ and $F \subset \partial K$ a mesh face satisfying Assumption* 4.6. *Define $T_F^K \subset K$ to be the simplex having F as a face and opposite vertex the point at distance h_F from F along the segment joining the barycenter of F with the center of star-shapedness of K. The face bubble function b_F is defined on K as the standard bubble function of T_F^K, cf.* [2, 35], *extended by zero to the rest of K.*

LEMMA 4.8. *Let $K \in \mathcal{T}$ and $F \subset \partial K$ be a mesh face under Assumption* 2.1. *Let $v \in \mathcal{P}_p(F)$ and denote by v also the constant extension in T_F^K of v in the direction normal to F. We have*

$$\|v\|_F^2 \le C_{b,F} \|b_F^{1/2} v\|_F^2, \tag{4.12}$$

with $C_{b,F} := [2(p+2)]^{2(d-1)} \frac{(d-1)^d}{(d-2)!}$, *and*

$$\|\nabla(b_F v)\|_{T_F^K}^2 \le C_{\mathrm{inv},T} h_K h_F^{-2} \|v\|_F^2, \tag{4.13}$$

with $C_{\mathrm{inv},T}$ the constant of the inverse inequality (4.1) *in the case of $d-1$-dimensional simplices. Moreover, we have*

$$\|\mathrm{curl}\,(b_T v)\|_{T_F^K}^2 \le (d-1) C_{\mathrm{inv},T} h_K h_F^{-2} \|v\|_F^2. \tag{4.14}$$

Proof. The bound (4.12) is given in [35] and (4.13) follows immediately from (4.1), the fact that $b_F \le 1$, and the fact that $\|v\|_{T_F^K}^2 \le h_K \|v\|_F^2$. Finally, the bound (4.14) is a trivial consequence of (4.13) observing once again that $\|\mathrm{curl}\, v\|_K^2 \le (d-1)\|\nabla v\|_K^2$. ∎

THEOREM 4.9 (flux residuals lower bound). *Let u be the solution of* (2.1) *and let $u_h \in S_{\mathcal{T}}$ be its dG approximation under Assumptions* 2.1, 2.3, *and* 4.6. *Then, for each $K \in \mathcal{T}$, we have*

(4.15)

$$\begin{aligned}
&\|h^{1/2} [\![a \nabla u_h \cdot \boldsymbol{n}]\!]\|_{\partial K \cap \Gamma_{\mathrm{int}}}^2 \\
&\quad \le 6 C_{b,F} \Bigg(2 C_{b,K} \big(\tau^2 + C_{\mathrm{inv},K}\big)(\alpha^*)^2 \|\sqrt{a} \nabla e\|_{\omega_K}^2 + \sum_{K' \in \omega_K} (1 + 2 C_{b,K}) O_{K',E}^2 \\
&\qquad + \alpha^* C_{\mathrm{inv},T} \sum_{F \in \partial K \cap \Gamma_{\mathrm{int}}} h_F^{-1} h_{F^\perp} \|\sqrt{a} \nabla e\|_{\omega_F}^2 \Bigg),
\end{aligned}$$

and

$$\|h^{1/2} [\![\nabla_{\mathrm{T}} u_h]\!]\|_{\Gamma_{\mathrm{int}}}^2 \le 2 C_{b,F} (d-1) \alpha_* C_{\mathrm{inv},T} \sum_{F \in \partial K \cap \Gamma_{\mathrm{int}}} h_F^{-1} h_{F^\perp} \|\sqrt{a} \nabla e\|_{\omega_F}^2; \tag{4.16}$$

here, ω_K is the patch of elements neighboring K, $\omega_F = T_F^K \cup T_F^{K'}$ with K' the element neighboring K across F and $h_{F^\perp} := \max\{h_K, h_{K'}\}$.

Proof. In view of proving (4.15), we first consider any $F \in \partial K$ with $F \in \Gamma_{\mathrm{int}}$. Further, we fix $v \in H^1(\omega_F)$ as the constant extension of $[\![a \nabla u_h \cdot \boldsymbol{n}]\!]|_F$ in the direction normal to F, so that $b_F v \in H_0^1(\omega_F)$; cf. Lemma 4.8. Then, testing the error equation (3.13) with $b_F v$ extended to zero on the whole of Ω, we get

$$\begin{aligned}
\int_{\omega_F} a \nabla_h e \cdot \nabla(b_F v)\,\mathrm{d}\mathbf{x} &= \int_{\omega_F} (f - \Pi f)(b_F v)\,\mathrm{d}\mathbf{x} + \int_{\omega_F} (\Pi f + \nabla \cdot (a \nabla u_h))(b_F v)\,\mathrm{d}\mathbf{x} \\
&\quad - \int_F [\![a \nabla u_h \cdot \boldsymbol{n}]\!]^2 b_F\,\mathrm{d}s.
\end{aligned}$$

From this, using (4.13) and the fact that $\|b_F v\|_K^2 = \|b_F v\|_{T_F^K}^2 \le h_K \|[\![a\nabla u_h \cdot \boldsymbol{n}]\!]\|_F^2$, the same bound being true on K', we obtain

$$\begin{aligned}\|[\![a\nabla u_h \cdot \boldsymbol{n}]\!] b_F^{1/2}\|_F^2 \le & \sum_{\mathcal{K}\in\{K,K'\}} \Big[(\|\Pi f - f\|_{T_F^{\mathcal{K}}} + \|(\Pi f + \nabla\cdot(a\nabla u_h))\|_{T_F^{\mathcal{K}}}) \|b_F v\|_{T_F^{\mathcal{K}}} \\ & + \|\sqrt{a}\nabla e\|_{T_F^{\mathcal{K}}} \|\sqrt{a}\nabla(b_F v)\|_{T_F^{\mathcal{K}}} \Big] \\ \le & \sum_{\mathcal{K}\in\{K,K'\}} \Big[h_{\mathcal{K}}^{1/2} (\|\Pi f - f\|_{T_F^{\mathcal{K}}} + \|(\Pi f + \nabla\cdot(a\nabla u_h))\|_{T_F^{\mathcal{K}}}) \\ & + (\alpha^* C_{\mathrm{inv},T} h_F^{-1} h_{\mathcal{K}})^{1/2} h_F^{-1/2} \|\sqrt{a}\nabla e\|_{T_F^{\mathcal{K}}} \Big] \|[\![a\nabla u_h \cdot \boldsymbol{n}]\!]\|_F.\end{aligned}$$

This, together with (4.12), gives

$$\begin{aligned}\|h^{1/2}[\![a\nabla u_h \cdot \boldsymbol{n}]\!]\|_F^2 \le 2C_{b,F} \sum_{\mathcal{K}\in\{K,K'\}} \Big[& (\|h(\Pi f - f)\|_{T_F^{\mathcal{K}}} + \|h(\Pi f + \nabla\cdot(a\nabla u_h))\|_{T_F^{\mathcal{K}}}) \\ & + (\alpha^* C_{\mathrm{inv},T})^{1/2} h_F^{-1} h_{\mathcal{K}} \|\sqrt{a}\nabla e\|_{T_F^{\mathcal{K}}} \Big]^2.\end{aligned}$$

Summing over all internal faces of K, noting carefully that the involved domains do not overlap, we finally obtain

$$\begin{aligned}\|h^{1/2}[\![a\nabla u_h \cdot \boldsymbol{n}]\!]\|_{\partial K\cap\Gamma_{\mathrm{int}}}^2 \le 6C_{b,F} \Big(& \|h(\Pi f - f)\|_{\omega_K}^2 + \|h(\Pi f + \nabla\cdot(a\nabla u_h))\|_{\omega_K}^2 \\ & + \alpha^* C_{\mathrm{inv},T} \sum_{F\in\partial K\cap\Gamma_{\mathrm{int}}} (h_F^{-1} h_{F^\perp})^2 \|\sqrt{a}\nabla e\|_{\omega_F}^2 \Big),\end{aligned} \tag{4.17}$$

as $h_{F^\perp} := \max\{h_K, h_{K'}\}$, from which (4.15) now follows by employing (4.10).

The proof concerning the tangential jump residual is similar. Given $F \in \Gamma_{\mathrm{int}}$, we fix $v \in H^1(\omega_F)$ as the constant extension of $[\![\nabla_{\mathrm{T}} u_h]\!]|_F$ in the direction normal to F, so that $b_F v \in H_0^1(\omega_F)$. Using the fact that $\operatorname{curl}\nabla u = \mathbf{0}$, we have the key observation

$$\int_{\omega_F} \operatorname{curl}(b_F v)\cdot\nabla u \,\mathrm{d}\mathbf{x} = 0. \tag{4.18}$$

Integration by parts and (4.14) give

$$\begin{aligned}\|[\![\nabla_{\mathrm{T}} u_h]\!] b_F^{1/2}\|_F^2 = \int_{\omega_F} \operatorname{curl}(b_F v)\cdot\nabla u_h \,\mathrm{d}\mathbf{x} &= \int_{\omega_F} \operatorname{curl}(b_F v)\cdot\nabla(u_h - u)\,\mathrm{d}\mathbf{x} \\ &\le \alpha_* \sum_{\mathcal{K}=K,K'} \|\sqrt{a}\nabla e\|_{T_F^{\mathcal{K}}} \|\operatorname{curl}(b_T v)\|_{T_F^{\mathcal{K}}} \\ &\le \alpha_* \big((d-1)C_{\mathrm{inv},T} h_{\mathcal{K}}\big)^{1/2} h_F^{-1} \|[\![\nabla_{\mathrm{T}} u_h]\!]\|_F \sum_{\mathcal{K}\in\{K,K'\}} \|\sqrt{a}\nabla e\|_{T_F^{\mathcal{K}}}.\end{aligned}$$

Hence, by using (4.12), we obtain

$$\|h^{1/2}[\![\nabla_{\mathrm{T}} u_h]\!]\|_F^2 \le 2\alpha_*(d-1)C_{\mathrm{inv},T} C_{b,F} (h_F^{-1} h_{F^\perp})^2 \|\sqrt{a}\nabla e\|_{\omega_F}^2.$$

The required lower bound on the jump of the tangential gradient now follows by summing over all internal faces belonging to K. ∎

By construction, we have $|\omega_F| \sim h_F^d$ for the patches ω_F. The terms involving norms over ω_F in Theorem 4.9 reflect and account for the presence of relatively small

faces. Indeed, linking the size of ω_F to that of F, instead of that of the element K, allows very large ratios h_K/h_F.

If, on the other hand, the size of each of the element's faces is comparable to that of the element itself, then we may modify the construction of the face bubble of Definition 4.7 by moving the opposite vertex all the way to the center of star-shapedness of K. In such a case, $h_F^{-1}h_{F^\perp}\|\sqrt{a}\nabla e\|_{\omega_F} \lesssim \|\sqrt{a}\nabla e\|_{K\cup K'}$. Thus, for meshes with potentially many but regular hanging nodes, the new flux-residuals' lower bounds revert to the classical ones, as encapsulated in the following corollary.

COROLLARY 4.10. *Under the assumption of Theorem* 4.9*, if, moreover, for every* $K \in \mathcal{T}$ *and* $F \in \partial K$ *it holds that* $h_F \geq \tau^{-1}h_K$*, then*

$$\begin{aligned}(4.19)\qquad &\|h^{1/2}[\![a\nabla u_h \cdot \boldsymbol{n}]\!]\|^2_{\partial K\cap\Gamma_{\text{int}}}\\ &\quad\leq 6C_{b,F}\Bigg((2C_{b,K}\big(\tau^2+C_{\text{inv},K}\big)(\alpha^*)^2+\tau\alpha^*C_{\text{inv},K})\|\sqrt{a}\nabla e\|^2_{\omega_K}\\ &\qquad+\sum_{K'\in\omega_K}(1+2C_{b,K})O^2_{K',E}\Bigg),\end{aligned}$$

and

$$(4.20)\qquad \|h^{1/2}[\![\nabla_{\mathrm{T}}u_h]\!]\|^2_{\partial K\cap\Gamma_{\text{int}}} \leq 2C_{b,F}(d-1)\tau\alpha_*C_{\text{inv},K}\|\sqrt{a}\nabla e\|^2_{\omega_K}.$$

Remark 4.11. Corollary 4.10 holds in the setting of fully shape-regular meshes allowing for the submesh auxiliary mesh construction; cf. section 2.3.1. Hence, Corollary 4.10 together with Theorem 4.5 and Theorem 3.5 establishes the reliability and efficiency of the classical residual error estimator for general fully shape-regular polytopic meshes with multiple hanging nodes. The analysis, also in this case, differs from the classical one in that the finite element space used to control the nonconforming error, being based on the auxiliary mesh, is *not* a subspace of the discrete solution space $S_{\mathcal{T}}$. Moreover, the resulting error bound is as explicit as the classical bound because, in this case, the auxiliary mesh quality is fully controlled by that of the polytopic mesh. The element bubble construction is also new and accounts for the polytopic nature of the mesh.

On the other hand, controlling the flux residuals in the extreme case of possibly unbounded non– shape-regular interfaces requires further new ideas. Whenever it is possible to construct a face bubble function b_F such that the bound

$$\|\nabla(b_Fv)\|^2_{T_F^K} \leq C_{\text{inv},T}h_K^{-1}\|v\|^2_F$$

holds true, the lower bounds of the flux residuals (4.15) and (4.16) will be independent of $h_F^{-1}h_{F^\perp}$. An alternative approach could be to consider bubble functions constructed on a neighboring set of structured elements. Then, the bubble functions b_F will be independent of the individual face size and the number of elements. For instance, this is the approach used in [36] to derive a lower bound of the flux residual of the FEM employing structured anisotropic triangular meshes. However, the construction of such face bubble functions for the general-shaped polytopic meshes considered in this work is highly nontrivial.

5. Numerical experiments. We present two numerical examples testing the new a posteriori error estimator. With the first example we test the impact of polygonal elements with a large number of small faces on the effectivity index. With the

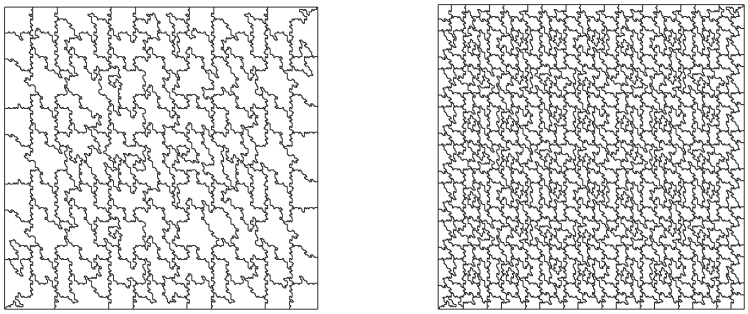

FIG. 6. *Example* 1. *Sample meshes with* 114 *(left) and* 498 *(right) polygonal elements obtained by agglomeration of a fine triangular mesh made of one million elements.*

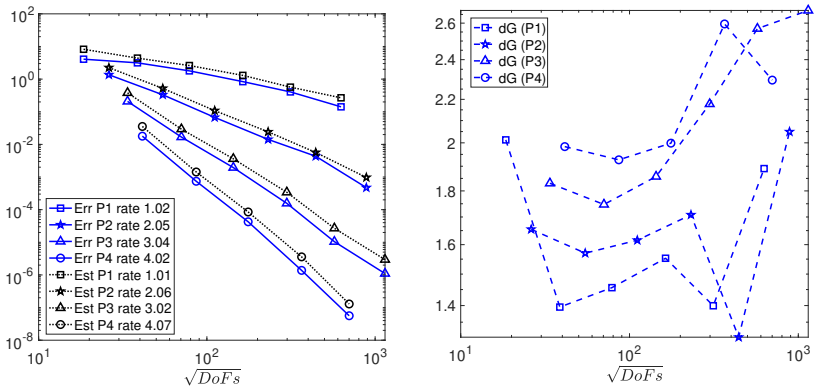

FIG. 7. *Example* 1. *Convergence history of the error and error estimator of* (3.21) *for* $p = 1, 2, 3, 4$ *(left) and respective effectivity measured as the ratio estimator over error (right).*

second, we test the performance of the estimator within a nonstandard adaptive algorithm. In all cases, we set $C_\sigma = 10$.

5.1. Example 1. We construct a sequence of polygonal meshes containing 114, 498, 2063, 8912, and 32768 elements obtained by successive agglomeration of a very fine triangular background mesh made of 10^6 elements. Each of the polygonal elements contains at least 50 edges; see Figure 6 for an illustration.

We consider the problem (2.1), with $a = I_{2\times 2}$ and $\Omega := (-1, 1)^2$. The Dirichlet boundary conditions and the source term f are determined by the exact solution $u = \sin(\pi x)\sin(\pi y)$. Numerical results for $p = 1, 2, 3, 4$ are displayed in Figure 7. The observed convergence rate of both the error and the estimator is $\mathcal{O}(DoFs^{-\frac{p}{2}})$, i.e., optimal in terms of the total number of degrees of freedom (DoFs). Moreover, the effectivity index is bounded between 1.2 and 2.6, hence showing that efficiency is not affected by the complexity of the element shapes. This numerical observation reflects that Assumption 4.6 may not be necessary.

Next, we compare the percentage contribution of the different components to the total estimator. Setting $R_X := (\sum_{K\in\mathcal{T}} R_{K,X}^2)^{1/2}$ for $X \in \{E, N, J, T\}$, in Table 1 we provide the percentage of total element residual R_E, total jump residual R_J, total

TABLE 1

Example 1. *Estimator's components percentage contributions to the dG error for* $p = 1, 2$*: element residual* R_E*, jump residual* R_J*, jump of the normal flux residual* R_N*, and jump of the tangential flux residual* R_T*.*

	$p=1$				$p=2$			
# elem	R_E	R_J	R_N	R_T	R_E	R_J	R_N	R_T
114	64%	18%	9%	9%	56%	26%	9%	9%
498	59%	23%	9%	9%	45%	36%	9%	10%
2063	36%	37%	13%	14%	45%	33%	10%	12%
8912	32%	37%	14%	17%	43%	31%	11%	15%

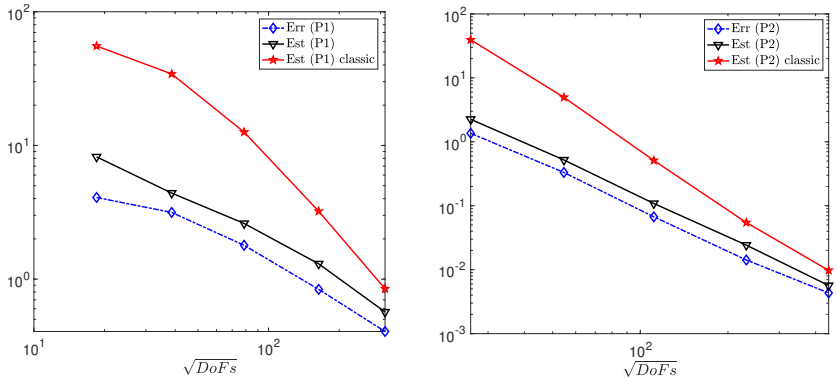

FIG. 8. *Example* 1. *Convergence history of the error, error estimator of* (3.21) *and the classical estimator for* $p = 1, 2$.

jump of the normal flux residual R_N, and total jump of the tangential flux residual R_T for $p = 1, 2$. For the coarse meshes of Figure 7, the element residual dominates the total estimator, followed by R_J. For finer meshes, we observe a significant contribution by R_E, R_J, and combined R_T and R_N.

Further, to highlight the importance of the presence of R_T in the new estimator presented in this work, we compare it to the a posteriori error estimator that can be derived using standard techniques from [35], which does not contain the tangential flux jump R_T. As already mentioned in Remark 3.4, it is immediate to bound $R_{K,T}$ from $R_{K,J}$ through an inverse estimate on each face F, giving $R_{K,T} \lesssim \frac{h_K}{\rho_F} R_{K,J}$, with ρ_F denoting the inscribed radius of the face F. Clearly, for small faces, we have $\rho_F \leq h_F \ll h_K$, showcasing that $R_{K,T}$ is theoretically sharper than $R_{J,T}$. In Figure 8, we present the error, the estimator from (3.21), and the *classic* estimator whereby $R_{K,T}$ is replaced by $\frac{h_K}{\rho_F} R_{K,J}$ for $p = 1, 2$. The superiority of the estimator presented in this work is evident for coarse meshes with large ratio $\frac{h_K}{h_F}$. We note that the jump terms account for more than 80% of the classical error estimator, thus indicating that the term $R_{J,T}$ is indeed responsible for the relative overestimation of the error. This confirms the theoretical intuition and showcases the practicality of the estimator proven in this work.

5.2. Example 2. We test a new adaptive algorithm driven by the error estimator from section 3. Starting from a relatively coarse simplicial mesh, we use the estimator (3.21) to mark simplicial elements for refinement through a bulk-chasing criterion (also

known as Dörfler marking), and also mark *pairs* of elements for agglomeration based on the size of the jump residual terms on elemental interfaces. Refinement of simplicial elements is performed via a newest vertex bisection algorithm. In the agglomeration step, general, polygonal meshes will be generated. In successive iterations, polygonal meshes which are marked for refinement are subdivided into either a finer polygonal mesh or a simplicial mesh, depending on their level of agglomeration. For simplicity, we do not consider the data oscillation terms. The adaptive algorithm can thus be described as

$$\text{SOLVE} \longrightarrow \text{ESTIMATE} \longrightarrow \text{MARK} \longrightarrow \text{REFINE/AGGLOMERATE}.$$

We consider the problem (2.1) with $a = I_{2\times 2}$ on $\Omega := (-1,1)^2 \setminus (0,1)\times(-1,0)$. The Dirichlet boundary conditions and the source term f are determined by the exact solution

$$u = r^{2/3}\sin(2\psi/3) + \exp(-1000((x-0.5)^2+(y-0.25)^2)) + \exp(-1000((x-0.5)^2+(y-0.75)^2)),$$

which has a point singularity at the origin. We test the adaptive dG algorithm described above with $p = 1,2,3$, with Dörfler's marking strategy 25% for refinement and the maximum marking strategy 5% for agglomeration. We point out that the agglomeration step is driven by the jump terms $R_{F,N}$, $R_{F,J}$, and $R_{F,T}$ for all faces $F \subseteq \partial K_i \cap \partial K_j$ on the meshes' interface between elements K_i and K_j.

The performance of the proposed adaptive algorithm is showcased in Figure 9. The convergence rates of both error and estimator are optimal in terms of the total number of DoFs, which is $\mathcal{O}(DoFs^{-\frac{p}{2}})$. Further, on coarse mesh levels, the mesh agglomeration dominates the mesh refinement. Consequently, the number of DoFs is initially reduced by the adaptive algorithm, while the error is also reduced. Another

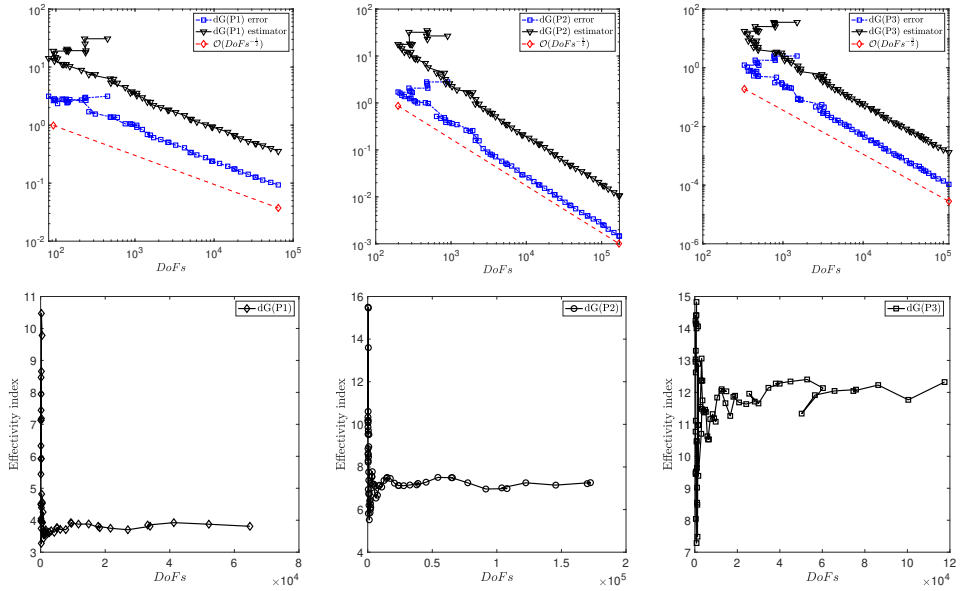

FIG. 9. *Error, estimator (top) and effectivity index (bottom) of the new adaptive polytopic dG method with* $p = 1,2,3$.

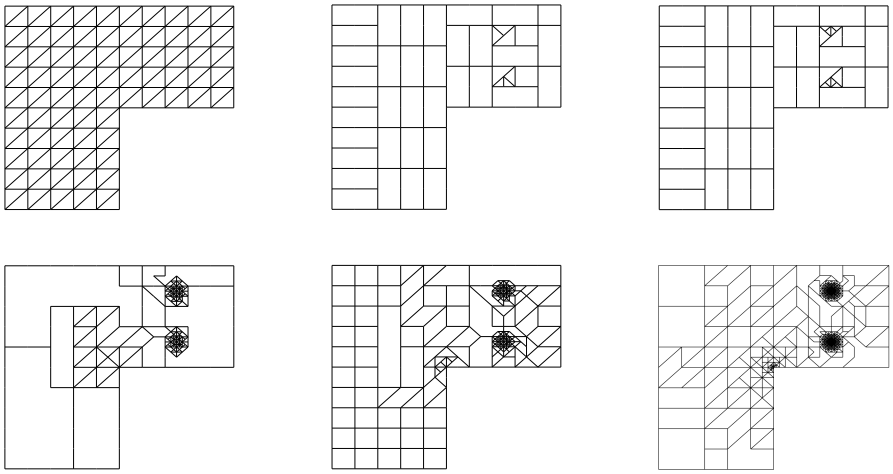

FIG. 10. *The sequence of meshes generated by the adaptive polytopic dG algorithm with* $p = 3$.

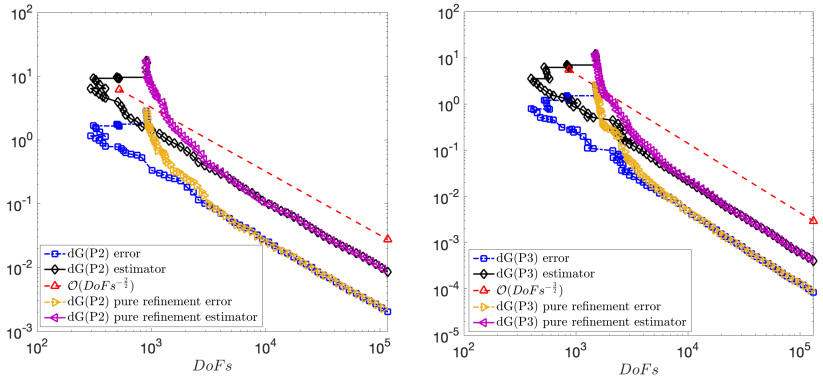

FIG. 11. *Example* 2. *Error and estimator of the new adaptive polytopic dG method and adaptive dG method without agglomeration for* $p = 2, 3$.

important observation is that the coarse mesh level's effectivity index still seems quite reasonable, namely 2 to 3 times greater than the asymptotic value. This is in spite of the presence of some very large polygonal elements next to small shape-regular triangles. These can be seen, for example, in the sequence of meshes produced by the adaptive algorithm with $p = 3$ shown in Figure 10.

Finally, we perform a comparison between the adaptive algorithm with and without agglomeration for $p = 2, 3$, using the same marking parameter and stopping criterion. The results are presented in Figure 11. Clearly, agglomeration helps reduce DoFs almost without influencing the accuracy on coarse meshes. As the meshes are refined, the advantage of polygonal elements is gradually reduced, as expected.

Acknowledgments. This research work was supported by the Hellenic Foundation for Research and Innovation (H.F.R.I.) under the "First Call for H.F.R.I. Research Projects to support Faculty members and Researchers and the procurement of high-cost research equipment grant" (Project Numbers: 3270, 1034 and 2152). Also, EHG wishes to acknowledge the financial support of The Leverhulme Trust (grant

number RPG-2021- 238) and of EPSRC (grant number EP/W005840/1). Finally, AC acknowledges the financial support of the MRC (grant number MR/T017988/1).

REFERENCES

[1] M. Ainsworth, *A posteriori error estimation for discontinuous Galerkin finite element approximation*, SIAM J. Numer. Anal., 45 (2007), pp. 1777–1798, https://doi.org/10.1137/060665993.

[2] M. Ainsworth and J. T. Oden, *A Posteriori Error Estimation in Finite Element Analysis*, Pure Appl. Math. (N. Y.), Wiley-Interscience, New York, 2000, https://doi.org/10.1002/9781118032824.

[3] M. Ainsworth and R. Rankin, *Fully computable error bounds for discontinuous Galerkin finite element approximations on meshes with an arbitrary number of levels of hanging nodes*, SIAM J. Numer. Anal., 47 (2010), pp. 4112–4141, https://doi.org/10.1137/080725945.

[4] D. N. Arnold, F. Brezzi, B. Cockburn, and L. D. Marini, *Unified analysis of discontinuous Galerkin methods for elliptic problems*, SIAM J. Numer. Anal., 39 (2002), pp. 1749–1779, https://doi.org/10.1137/S0036142901384162.

[5] F. Bassi, L. Botti, A. Colombo, and S. Rebay, *Agglomeration based discontinuous Galerkin discretization of the Euler and Navier-Stokes equations*, Comput. & Fluids, 61 (2012), pp. 77–85, https://doi.org/10.1016/j.compfluid.2011.11.002.

[6] R. Becker, P. Hansbo, and M. G. Larson, *Energy norm a posteriori error estimation for discontinuous Galerkin methods*, Comput. Methods Appl. Mech. Engrg., 192 (2003), pp. 723–733, https://doi.org/10.1016/S0045-7825(02)00593-5.

[7] F. Bertrand, C. Carstensen, B. Gräßle, and N. T. Tran, *Stabilization-free HHO a posteriori error control*, Numer. Math., 154 (2023), pp. 369–408, https://doi.org/10.1007/s00211-023-01366-8.

[8] A. Bonito and R. H. Nochetto, *Quasi-optimal convergence rate of an adaptive discontinuous Galerkin method*, SIAM J. Numer. Anal., 48 (2010), pp. 734–771, https://doi.org/10.1137/08072838X.

[9] Z. Cai, X. Ye, and S. Zhang, *Discontinuous Galerkin finite element methods for interface problems: A priori and a posteriori error estimations*, SIAM J. Numer. Anal., 49 (2011), pp. 1761–1787, https://doi.org/10.1137/100805133.

[10] A. Cangiani, Z. Dong, and E. Georgoulis, *hp-version discontinuous Galerkin methods on essentially arbitrarily-shaped elements*, Math. Comp., 91 (2022), pp. 1–35, https://doi.org/10.1090/mcom/3667.

[11] A. Cangiani, Z. Dong, and E. H. Georgoulis, *hp-version space-time discontinuous Galerkin methods for parabolic problems on prismatic meshes*, SIAM J. Sci. Comput., 39 (2017), pp. A1251–A1279, https://doi.org/10.1137/16M1073285.

[12] A. Cangiani, Z. Dong, E. H. Georgoulis, and P. Houston, *hp-Version Discontinuous Galerkin Methods on Polygonal and Polyhedral Meshes*, Springer, New York, 2017.

[13] A. Cangiani, E. H. Georgoulis, and P. Houston, *hp-version discontinuous Galerkin methods on polygonal and polyhedral meshes*, Math. Models Methods Appl. Sci., 24 (2014), pp. 2009–2041, https://doi.org/10.1142/S0218202514500146.

[14] A. Cangiani, E. H. Georgoulis, T. Pryer, and O. J. Sutton, *A posteriori error estimates for the virtual element method*, Numer. Math., 137 (2017), pp. 857–893, https://doi.org/10.1007/s00211-017-0891-9.

[15] A. Cangiani, E. H. Georgoulis, and O. J. Sutton, *Adaptive non-hierarchical Galerkin methods for parabolic problems with application to moving mesh and virtual element methods*, Math. Models Methods Appl. Sci., 31 (2021), pp. 711–751, https://doi.org/10.1142/S0218202521500172.

[16] C. Carstensen, S. Bartels, and S. Jansche, *A posteriori error estimates for nonconforming finite element methods*, Numer. Math., 92 (2002), pp. 233–256, https://doi.org/10.1007/s002110100378.

[17] C. Carstensen and S. A. Funken, *Constants in Clément-interpolation error and residual based a posteriori error estimates in finite element methods*, East-West J. Numer. Math., 8 (2000), pp. 153–175.

[18] C. Carstensen, T. Gudi, and M. Jensen, *A unifying theory of a posteriori error control for discontinuous Galerkin FEM*, Numer. Math., 112 (2009), pp. 363–379, https://doi.org/10.1007/s00211-009-0223-9.

[19] C. Carstensen, R. Khot, and A. K. Pani, *A priori and a posteriori error analysis of the lowest-order NCVEM for second-order linear indefinite elliptic problems*, Numer. Math., 151 (2022), pp. 551–600.

[20] L. P. Chew, *Constrained Delaunay triangulations*, Algorithmica, 4 (1989), pp. 97–108, https://doi.org/10.1007/BF01553881.

[21] J. Cui, F. Gao, Z. Sun, and P. Zhu, *A posteriori error estimate for discontinuous Galerkin finite element method on polytopal mesh*, Numer. Methods Partial Differential Equations, 36 (2020), pp. 601–616, https://doi.org/10.1002/num.22443.

[22] E. Dari, R. Duran, C. Padra, and V. Vampa, *A posteriori error estimators for nonconforming finite element methods*, ESAIM Math. Model. Numer. Anal., 30 (1996), pp. 385–400.

[23] A. Demlow and E. H. Georgoulis, *Pointwise a posteriori error control for discontinuous Galerkin methods for elliptic problems*, SIAM J. Numer. Anal., 50 (2012), pp. 2159–2181, https://doi.org/10.1137/110846397.

[24] D. A. Di Pietro and R. Specogna, *An a posteriori-driven adaptive mixed high-order method with application to electrostatics*, J. Comput. Phys., 326 (2016), pp. 35–55, https://doi.org/10.1016/j.jcp.2016.08.041.

[25] Z. Dong and E. H. Georgoulis, *Robust interior penalty discontinuous Galerkin methods*, J. Sci. Comput., 92 (2022), 57, https://doi.org/10.1007/s10915-022-01916-6.

[26] H. Edelsbrunner, *Geometry and Topology for Mesh Generation*, Cambridge Monographs on Applied and Computational Mathematics, Cambridge University Press, Cambridge, UK, 2001.

[27] S. R. Elias, G. D. Stubley, and G. D. Raithby, *An adaptive agglomeration method for additive correction multigrid*, Internat. J. Numer. Methods Engrg., 40 (1997), pp. 887–903.

[28] A. Ern and M. Vohralík, *Polynomial-degree-robust a posteriori estimates in a unified setting for conforming, nonconforming, discontinuous Galerkin, and mixed discretizations*, SIAM J. Numer. Anal., 53 (2015), pp. 1058–1081, https://doi.org/10.1137/130950100.

[29] E. H. Georgoulis and A. Lasis, *A note on the design of hp-version interior penalty discontinuous Galerkin finite element methods for degenerate problems*, IMA J. Numer. Anal., 26 (2006), pp. 381–390, https://doi.org/10.1093/imanum/dri038.

[30] S. Giani and P. Houston, *hp-adaptive composite discontinuous Galerkin methods for elliptic problems on complicated domains*, Numer. Methods Partial Differential Equations, 30 (2014), pp. 1342–1367, https://doi.org/10.1002/num.21872.

[31] V. Girault and P. A. Raviart, *Finite Element Methods for Navier-Stokes Equations: Theory and Algorithms*, Springer Ser. Comput. Math. 5, Springer-Verlag, Berlin, 1986, https://doi.org/10.1007/978-3-642-61623-5.

[32] R. H. W. Hoppe, G. Kanschat, and T. Warburton, *Convergence analysis of an adaptive interior penalty discontinuous Galerkin method*, SIAM J. Numer. Anal., 47 (2008), pp. 534–550, https://doi.org/10.1137/070704599.

[33] P. Houston, D. Schötzau, and T. P. Wihler, *Energy norm a posteriori error estimation of hp-adaptive discontinuous Galerkin methods for elliptic problems*, Math. Models Methods Appl. Sci., 17 (2007), pp. 33–62, https://doi.org/10.1142/S0218202507001826.

[34] O. A. Karakashian and F. Pascal, *Convergence of adaptive discontinuous Galerkin approximations of second-order elliptic problems*, SIAM J. Numer. Anal., 45 (2007), pp. 641–665, https://doi.org/10.1137/05063979X.

[35] O. A. Karakashian and F. Pascal, *A posteriori error estimates for a discontinuous Galerkin approximation of second-order elliptic problems*, SIAM J. Numer. Anal., 41 (2003), pp. 2374–2399, https://doi.org/10.1137/S0036142902405217.

[36] N. Kopteva, *Lower a posteriori error estimates on anisotropic meshes*, Numer. Math., 146 (2020), pp. 159–179, https://doi.org/10.1007/s00211-020-01137-9.

[37] C. Kreuzer and E. H. Georgoulis, *Convergence of adaptive discontinuous Galerkin methods*, Math. Comp., 87 (2018), pp. 2611–2640, https://doi.org/10.1090/mcom/3318.

[38] C. Kreuzer and A. Veeser, *Oscillation in a posteriori error estimation*, Numer. Math., 148 (2021), pp. 43–78, https://doi.org/10.1007/s00211-021-01194-8.

[39] H. Li, L. Mu, and X. Ye, *A posteriori error estimates for the weak Galerkin finite element methods on polytopal meshes*, Commun. Comput. Phys., 26 (2019), pp. 558–578, https://doi.org/10.4208/cicp.oa-2018-0058.

[40] M. M. Corti, P. Antonietti, L. Dedé, and A. Quarteroni, *Numerical Modelling of the Brain Poromechanics by High-Order Discontinuous Galerkin Methods*, arXiv:2210.02272, 2022.

[41] J. M. Melenk, *hp-interpolation of nonsmooth functions and an application to hp-a posteriori error estimation*, SIAM J. Numer. Anal., 43 (2005), pp. 127–155, https://doi.org/10.1137/S0036142903432930.

[42] L. R. Scott and S. Zhang, *Finite element interpolation of nonsmooth functions satisfying boundary conditions*, Math. Comp., 54 (1990), pp. 483–493, https://doi.org/10.2307/2008497.

[43] J. R. Shewchuk, *A condition guaranteeing the existence of higher-dimensional constrained Delaunay triangulations*, in Proceedings of the Fourteenth Annual Symposium on Computational Geometry, ACM, New York, 1998, pp. 76–85.

[44] J. R. Shewchuk, *General-dimensional constrained Delaunay and constrained regular triangulations.* I. *Combinatorial properties*, Discrete Comput. Geom., 39 (2008), pp. 580–637, https://doi.org/10.1007/s00454-008-9060-3.

[45] I. Smears, *Nonoverlapping domain decomposition preconditioners for discontinuous Galerkin approximations of Hamilton-Jacobi-Bellman equations*, J. Sci. Comput., 74 (2018), pp. 145–174, https://doi.org/10.1007/s10915-017-0428-5.

[46] S. K. Tomar and S. I. Repin, *Efficient computable error bounds for discontinuous Galerkin approximations of elliptic problems*, J. Comput. Appl. Math., 226 (2009), pp. 358–369, https://doi.org/10.1016/j.cam.2008.08.015.

[47] A. Veeser and R. Verfürth, *Poincaré constants for finite element stars*, IMA J. Numer. Anal., 32 (2012), pp. 30–47, https://doi.org/10.1093/imanum/drr011.

[48] R. Verfürth, *Error estimates for some quasi-interpolation operators*, M2AN Math. Model. Numer. Anal., 33 (1999), pp. 695–713, https://doi.org/10.1051/m2an:1999158.

[49] R. Verfürth, *A Posteriori Error Estimation Techniques for Finite Element Methods*, Numer. Math. Sci. Comput., Oxford University Press, Oxford, UK, 2013, https://doi.org/10.1093/acprof:oso/9780199679423.001.0001.

[50] W. Zheng and H. Qi, *On Friedrichs–Poincaré-type inequalities*, J. Math. Anal. Appl., 304 (2005), pp. 542–551, https://doi.org/10.1016/j.jmaa.2004.09.066.